HEPATOLOGY
Official Journal of the American Association for the Study of Liver Diseases

Adenosine Kinase Is a Key Determinant for the Anti-HCV Activity of Ribavirin

Kyoko Mori,[1] Osamu Hiraoka,[2] Masanori Ikeda,[1] Yasuo Ariumi,[1] Akiko Hiramoto,[3] Yusuke Wataya,[3] and Nobuyuki Kato[1]

Ribavirin (RBV) is often used in conjunction with interferon-based therapy for patients with chronic hepatitis C. There is a drastic difference in the anti–hepatitis C virus (HCV) activity of RBV between the HuH-7-derived assay system, OR6, possessing the RBV-resistant phenotype (50% effective concentration [EC_{50}]: >100 μM) and the recently discovered Li23-derived assay system, ORL8, possessing the RBV-sensitive phenotype (EC_{50}: 8 μM; clinically achievable concentration). This is because the anti-HCV activity of RBV was mediated by the inhibition of inosine monophosphate dehydrogenase in RBV-sensitive ORL8 cells harboring HCV RNA. By means of comparative analyses using RBV-resistant OR6 cells and RBV-sensitive ORL8 cells, we tried to identify host factor(s) determining the anti-HCV activity of RBV. We found that the expression of adenosine kinase (ADK) in ORL8 cells was significantly higher than that in RBV-resistant OR6 cells harboring HCV RNA. Ectopic ADK expression in OR6 cells converted them from an RBV-resistant to an RBV-sensitive phenotype, and inhibition of ADK abolished the activity of RBV. We showed that the differential ADK expression between ORL8 and OR6 cells was not the result of genetic polymorphisms in the ADK gene promoter region and was not mediated by a microRNA control mechanism. We found that the 5' untranslated region (UTR) of ADK messenger RNA in ORL8 cells was longer than that in OR6 cells, and that only a long 5' UTR possessed internal ribosome entry site (IRES) activity. Finally, we demonstrated that the long 5' UTR functioned as an IRES in primary human hepatocytes. *Conclusion*: These results indicate that ADK acts as a determinant for the activity of RBV and provide new insight into the molecular mechanism underlying differential drug sensitivity. (HEPATOLOGY 2013;58:1236-1244)

See Editorial on Page 1203

Hepatitis C virus (HCV) is an enveloped RNA virus, the genome of which consists of a positive-stranded 9.6-kilobase (kb) RNA encoding 10 structural and nonstructural (NS) proteins.[1] The combination of pegylated-interferon (Peg-IFN) and ribavirin (RBV) was the standard treatment for patients with chronic hepatitis C (CHC) until last year, when a new triple-agent combination therapy using an inhibitor of HCV NS3-4A protease (i.e., either telaprevir or boceprevir), in combination with Peg-IFN and RBV, was started.[2] The sustained virologic response (SVR) rate of genotype 1 using this new therapy is expected to increase from 55% to more than 70%.[3] However, there has also been an increase in side effects by RBV in the triple therapy, including several severe side effects, such as skin rash by telaprevir, ageusia by boceprevir, and advanced anemia by telaprevir/boceprevir.[3,4]

Abbreviations: Abs, antibodies; ADK, adenosine kinase; 5azaC, 5-azacytidine; CC_{50}, 50% cytotoxic concentration; cDNA, complementary DNA; CHC, chronic hepatitis C; EC_{50}, 50% effective concentration; GTP, guanosine triphosphate; HCV, hepatitis C virus; HPLC, high-performance liquid chromatography; IMPDH, inosine monophosphate dehydrogenase; IMP, inosine-5'-monophosphate; IRES, internal ribosome entry site; kb, kilobase; mRNA, messenger RNA; NS, nonstructural protein; nt, nucleotide; ORF, open reading frame; 4-PBA, 4-phenylbutyric acid; Peg-IFN, pegylated-interferon; PHHs, primary human hepatocytes; RACE, rapid amplification of cDNA ends; RBV, ribavirin; RL, renilla luciferase; RMP, RBV 5'-monophosphate; RT-PCR, reverse transcription-polymerase chain reaction; siRNA, small interfering RNA; miRNAs, microRNAs; SNP, single-nucleotide polymorphism; SVR, sustained virologic response; UTR, untranslated region.

From the [1]Department of Tumor Virology, Okayama University Graduate School of Medicine, Dentistry, and Pharmaceutical Sciences, Okayama, Japan; [2]School of Pharmacy, Shujitsu University, Okayama, Japan; and [3]Department of Drug Informatics, Faculty of Pharmaceutical Sciences, Okayama University, Okayama, Japan.

Received November 6, 2012; accepted March 19, 2013.

This work was supported by a grant-in-aid for research on hepatitis from the Ministry of Health, Labor and Welfare of Japan.

The main hurdle to resolving the side-effect profile is that the anti-HCV mechanism of RBV is not well understood, although several possible mechanisms have been proposed.[5,6] To date, there has been no cell-culture system enabling analysis of the anti-HCV mechanism of RBV at clinically achievable concentrations (5-14 μM), because the human hepatoma cell line, HuH-7, which has been the only cell line available for robust HCV replication, is not sensitive to RBV.[5,7,8] Indeed, we also observed that the 50% effective concentration (EC_{50}) of RBV against HCV RNA replication in our developed HuH-7-derived assay system (OR6), in which the genome-length HCV RNA (O strain of genotype 1b) encoding renilla luciferase (RL) replicates efficiently, was more than 100 μM, and 50% cytotoxic concentration (CC_{50}) was also more than 100 μM.[9,10]

On the other hand, we recently found that a new human hepatoma cell line, Li23, whose gene expression profile was distinct from that of HuH-7, enabling efficient HCV RNA replication and persistent HCV production, was sensitive to RBV.[10-12] Indeed, the EC_{50} value of RBV against HCV RNA replication in our developed Li23-derived assay system (ORL8), which is comparable to the OR6 assay system, was 8.7 μM, and the CC_{50} value was more than 100 μM.[10] It was noteworthy that this EC_{50} value was equivalent to the clinically achievable concentrations of RBV. Therefore, this finding led us to analyze the anti-HCV mechanism of RBV, and, consequently, we found that the anti-HCV activity of RBV was mediated by the inhibition of inosine monophosphate dehydrogenase (IMPDH), and that IMPDH was required for HCV RNA replication.[10]

From these findings, we anticipated that the comparative analysis of RBV-sensitive ORL8 cells and RBV-resistant OR6 cells would lead to the identification of host factor(s) determining the anti-HCV activity of RBV. Here, we report the finding that adenosine kinase (ADK) is an essential determinant of the anti-HCV activity of RBV.

Materials and Methods

Cell Cultures. HuH-7- and Li23-derived cells and PH5CH8 cells were maintained as described previously.[11] HT17 cells were cultured in Dulbecco's modified Eagle's medium supplemented with 10% fetal bovine serum. Primary human hepatocytes (PHHs; PhoenixBio, Higashihiroshima, Japan) were also maintained in the medium for the Li23-derived cells.

Reagents. RBV was kindly provided by Yamasa (Chiba, Japan).

Inosine-5'-monophosphate (IMP) and nucleoside triphosphates (cytidine triphosphate, uridine triphosphate, adenosine triphosphate, and guanosine triphosphate [GTP]) were also purchased from Yamasa. ABT-702 was purchased from Calbiochem (San Diego, CA). 5-azacytidine (5azaC) and 4-phenylbutyric acid (4-PBA) were purchased from Sigma-Aldrich (St. Louis, MO).

Western Blotting Analysis. Preparation of cell lysates, sodium dodecyl sulfate polyacrylamide gel electrophoresis, and immunoblotting analysis were performed as previously described.[13] Polyclonal-ADK (ab54818; Abcam, Cambridge, MA), monoclonal-ADK (F-5; Santa Cruz Biotechnology, Santa Cruz, CA), and β-actin (AC-15; Sigma-Aldrich) antibodies (Abs) were used.

Reverse-Transcription Polymerase Chain Reaction. Reverse-transcription polymerase chain reaction (RT-PCR) was performed to detect ADK messenger RNA (mRNA), as described previously,[14] using the primer sets (ADKF and ADKR; ADK-5'-untranslated region [UTR]-187nts and ADK-5'-UTR checkR) listed in Supporting Table 1.

Quantitative RT-PCR. Quantitative RT-PCR analysis for ADK mRNA was performed using a real-time LightCycler PCR (Roche Diagnostics, Indianapolis, IN), as described previously,[11] with the primer sets (ADKF and ADKR; ADK-5'UTR-384nts and ADK-5'UTR checkR; ADK-5'UTR-318nts and ADK-5'UTR checkR; ADK-5'UTR-187nts and ADK-5'UTR checkR; ADK-5'UTR-125nts and ADK-5'UTR checkR) listed in Supporting Table 1.

RL Assay. RL assay was performed as described previously.[9] Experiments were performed at least in triplicate.

High-Performance Liquid Chromatography Analysis. Quantitative high-performance liquid chromatography (HPLC) analysis was performed using the

Address reprint requests to: Nobuyuki Kato, Ph.D., Department of Tumor Virology, Okayama University Graduate School of Medicine, Dentistry, and Pharmaceutical Sciences, 2-5-1 Shikata-cho, Okayama 700-8558, Japan. E-mail: nkato@md.okayama-u.ac.jp; fax: (81)86-235-7392.

View this article online at wileyonlinelibrary.com.

DOI 10.1002/hep.26421

Potential conflict of interest: Nothing to report.

Additional Supporting Information may be found in the online version of this article.

extract from the OR6 or ORL8 cells treated with 50 μM of RBV for 8 hours. HPLC analysis was performed as described previously.[15]

RNA Interference. Small interfering RNA (siRNA) duplexes targeting the coding regions of human ADK (catalog no.: M-009687-01; Dharmacon, Inc., Lafayette, CO) were chemically synthesized. A nontargeting siRNA duplex (catalog no.: D-001206-13; Dharmacon) was also used as a control. ORL8 cells were transfected with the indicated siRNA duplexes using Oligofectamine (Invitrogen, Carlsbad, CA).[10]

Ectopic Expression of ADK. The methods of plasmid construction for ectopic expression of ADK and retroviral infection using the constructed plasmids are described in the Supporting Materials.

Plasmid Construction and Internal Ribosome Entry Site Activity Assay. The method of plasmid construction for internal ribosome entry site (IRES) activity assay is described in the Supporting Materials. The dual luciferase reporter assay for IRES activity was performed by the method described previously.[14]

Statistical Analysis. Data are presented as means ± standard deviation. The Student unpaired *t* test was performed for statistical analysis between the two groups, and the difference was considered significant at $P < 0.05$.

Results

High Expression Level of ADK in ORL8 Cells. To identify the host factor responsible for the difference in RBV responses between Li23-derived ORL8 and HuH-7-derived OR6 cells, we first recompared the previous data from complementary DNA (cDNA) microarrays using Li23 and HuH-7 cells. Although we assigned 17 genes that showed dramatic differences in expression between Li23 and HuH-7 cells,[12] none of these genes were considered to be involved in the response to RBV. Expression of IMPDH1 (NM_000883) and IMPDH2 (NM_000884), which were involved in the anti-HCV mechanism of RBV,[8,10] was also at a similar level between Li23 and HuH-7 cells or between cured ORL8 (ORL8c) and cured OR6 (OR6c) cells (Supporting Table 2).

We next attempted to verify the process of GTP reduction that is expected to occur after RBV is incorporated into cells. To this end, we performed a quantitative HPLC analysis using the extract from the OR6 or ORL8 cells treated with 50 μM of RBV for 8 hours, which is the working time of RBV against HCV RNA replication.[10] Amounts of IMP and GTP were calculated from the peak area obtained by HPLC

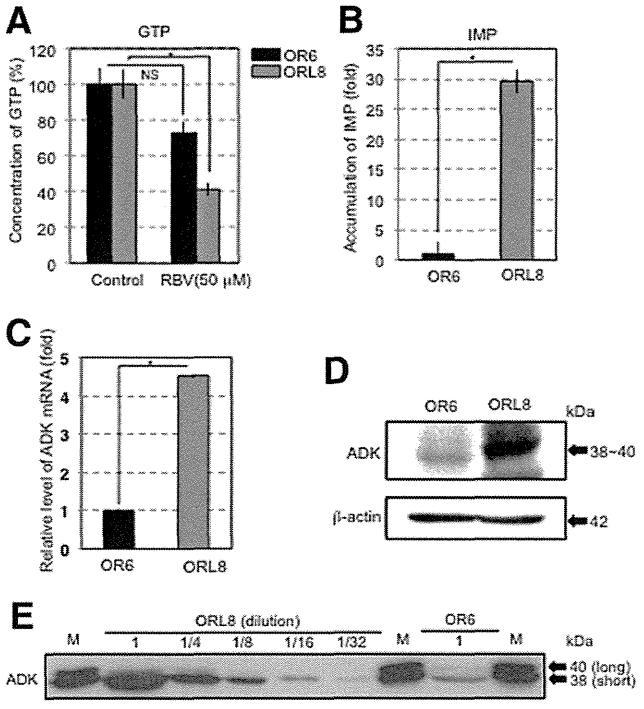

Fig. 1. Expression level of ADK in ORL8 cells was higher than that in OR6 cells. (A) Signal of GTP obtained by HPLC analysis using nts extracted from RBV-treated cells was quantified. (B) Signal of IMP obtained by HPLC analysis using nts extracted from RBV-treated cells was quantified. (C) Expression level of ADK mRNA in ORL8 cells was compared with that in OR6 cells by quantitative RT-PCR analysis. (D) Level of ADK in ORL8 cells was compared with that in OR6 cells by western blotting analysis. (E) ORL8 cell extract was diluted and then western blotting analysis was performed for the detection of ADK. Two isoforms of ADK (40 and 38 kDa) were loaded as molecular markers. Experiments (A-C) were performed in triplicate. $^*P < 0.05$; NS, not significant.

analysis. Volume of cells was calculated from the mean diameter of cells, and we found 10^6 cells to be equivalent to 1.1 mm^3. We assumed that the extracted nucleotides (nts) were uniformly distributed in the cell aqueous volume. As expected, the level of intracellular GTP in ORL8 cells showed a significant (60%) reduction, whereas that in OR6 cells showed only a 27% reduction (Fig. 1A and Supporting Fig. 1A-D). These results support our previous finding that the inhibitory effect of RBV on HCV RNA replication in ORL8 cells is stronger than that in OR6 cells.[10]

In addition, we noticed an unexpected phenomenon: A substantial accumulation of IMP occurred as the result of IMPDH inhibition in ORL8 cells, but not in OR6 cells. The IMP level in ORL8 cells became approximately 30 times higher than that in OR6 cells (Fig. 1B and Supporting Fig. 1A-D). However, no additive effect of inosine (up to 100 μM) on HCV RNA replication in ORL8 cells was observed (Supporting Fig. 2).

It has been reported that RBV is metabolized *in vivo* through RBV 5'-monophosphate (RMP), a

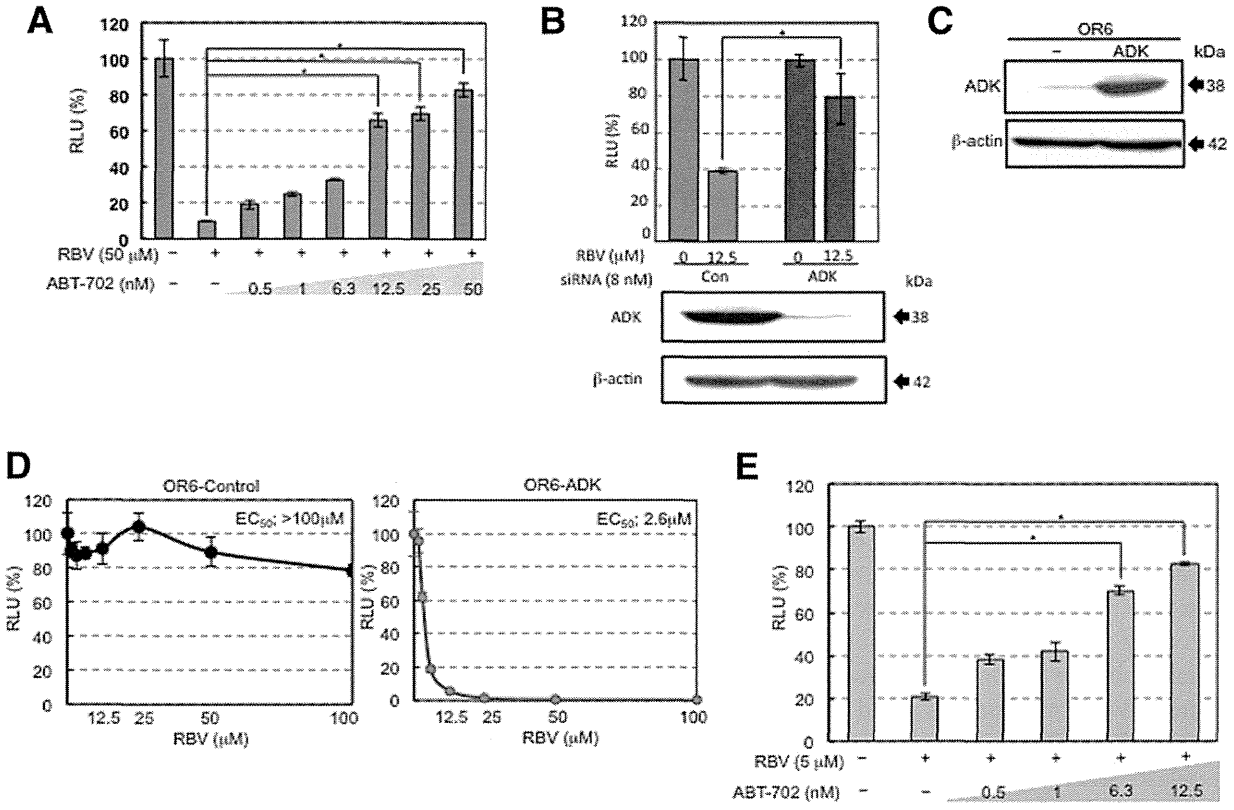

Fig. 2. ADK is a determining host factor for the anti-HCV activity of RBV. (A) ORL8 cells were cotreated with RBV (50 μM) and ABT-702 (nM) for 72 hours, after which an RL assay was performed. Relative luciferase activity (RLU) (%) calculated at each time point, when the level of luciferase activity in nontreated cells was assigned to be 100%, is shown. (B) ORL8 cells were transfected with 8 nM of siRNA targeting ADK. After 72 hours, expression levels of ADK were monitored by western blotting analysis (lower panel). ADK-knockdown ORL8 cells were treated with 12.5 μM of RBV for 72 hours, after which an RL assay was performed, as described in (A, upper panel). (C) Expression level of ADK in OR6-ADK cells was monitored by western blotting analysis. (D) OR6-ADK cells were treated with RBV for 72 hours and then an RL assay was performed as described in (A). (E) OR6-ADK cells were cotreated with RBV (5 μM) and ABT-702 (nM) for 72 hours and then an RL assay was performed, as described in (A). Experiments (A, B, D, and E) were performed in triplicate. $*P < 0.05$.

competitive inhibitor of IMPDH, by ADK.[16] Based on our findings, we expected that ADK activity might be able to control the anti-HCV activity of RBV. Indeed, microarray analysis revealed that the actual expression levels of ADK were 764 and 2,840 in OR6c and ORL8c cells, respectively. Quantitative RT-PCR analysis also showed that the mRNA level of ADK in ORL8 cells was 4.5 times higher than that in OR6 cells (Fig. 1C). Furthermore, we found that the protein level of ADK in ORL8 cells was much higher than that in OR6 cells (Fig. 1D).

On the other hand, it is known that ADK has two major isoforms: ADK-long (NM_006721) localized in the nucleus and ADK-short (NM_001123) localized in the cytoplasm.[17] ADK-long differs in the 5' UTR and initiates translation at an alternative start codon, compared to ADK-short. ADK-long is 17 amino acids longer than ADK-short. We prepared ORL8 cells stably overexpressing ORL8-derived ADK-long or ADK-short using a retroviral gene transfer system and examined its mobility in western blotting analysis. Fortunately, two isoforms were discriminable as 40 (ADK-long) and 38 kDa (ADK-short) (Fig. 1E). Using these isoforms as molecular markers, we performed semiquantitative western blotting analysis by the sample dilution method. The results revealed that the expression level of ADK-short in ORL8 cells was approximately 16 times higher than that in OR6 cells, and that ADK-long was little expressed in both cells (Fig. 1E). From these results, we assumed that the differences in ADK expression were involved in the dramatic differences in RBV sensitivity between the two cell lines. To address this assumption, we focused on the ADK-short in the following study; hereafter, ADK-short is designated as ADK.

ADK Is a Host Factor Determining the Anti-HCV Activity of RBV. To evaluate the hypothesis that ADK controls the anti-HCV activity of RBV, we first examined the effect of ABT-702, an ADK inhibitor, on the anti-HCV activity of RBV. The results revealed that ABT-702 cancelled the activity of RBV in ORL8

cells in a dose-dependent manner (Fig. 2A). Furthermore, we demonstrated that the activity of RBV was cancelled in ADK-knockdown ORL8 cells (Fig. 2B). These results suggest that the inhibition of ADK in ORL8 cells converts them from an RBV-sensitive phenotype to an RBV-resistant phenotype.

To directly demonstrate the involvement of ADK, we first prepared OR6 cells stably expressing ADK (OR6-ADK) (Fig. 2C). We were able to demonstrate that the OR6-ADK cells were dramatically converted from an RBV-resistant phenotype with an EC_{50} value of more than 100 μM to an RBV-sensitive phenotype with an EC_{50} value of 2.6 μM (Fig. 2D). We next examined whether or not the GTP reduction or IMP accumulation observed in ORL8 cells treated with RBV (Fig. 1A,B) occurs in OR6-ADK cells. The results revealed that the GTP reduction and IMP accumulation in RBV-treated OR6-ADK cells were more pronounced than in RBV-treated ORL8 cells (Supporting Fig. 3A,B). Because OR6 is a clonal cell line harboring genome-length HCV RNA, we used a polyclonal cell line (sOR) harboring HCV replicon RNA[9] to prepare sOR-ADK cells stably expressing ADK (Supporting Fig. 3C) and examined their sensitivity to RBV. sOR-ADK cells were also dramatically converted from an RBV-resistant phenotype with an EC_{50} value of more than 100 μM to an RBV-sensitive phenotype with an EC_{50} value of 6.0 μM (Supporting Fig. 3D). In addition, ORL8-ADK cells stably overexpressing ADK also showed EC_{50} values ranging from 13.2 to 1.2 μM (Supporting Fig. 3E). Furthermore, we demonstrated that the anti-HCV activity detected in OR6-ADK cells was also cancelled by ABT-702 treatment in a dose-dependent manner (Fig. 2E). Considering these results together, we conclude that ADK is a key determinant for the anti-HCV activity of RBV.

The Suppression of ADK Expression in OR6 Cells Was Not the Result of Genetic Variations or Epigenetic Alterations in the ADK Gene Promoter. To clarify the mechanism underlying the difference in ADK expression between OR6 and ORL8 cells, we first examined the nt sequences of up to several kb upstream from the transcription start point estimated from NM_001123 (31-OCT-2010) using the data of AL731576. Several possible transcription elements, such as the GC box (−12 and −187 of ADK gene), p53 response element (−252 and −585), and heat shock element (−559, −971, −1486, and −1797) were detected in up to approximately 2 kb upstream from the estimated transcription start point, but not in more 2 kb. Accordingly, we amplified approximately 2 kb including the 5' UTR (187 nts estimated by NM_001123 [31-OCT-2010]) by PCR using DNA prepared from ORL8 or OR6 cells, and each PCR product was inserted into pGL4.10-luc2 for the sequence analysis and reporter analysis of gene promoter activity. Sequence analysis confirmed that the sequences of the inserts were the same as the sequence data of the ADK gene (AL731576), except in the case of a single-nucleotide polymorphism (SNP) [rs10824095; C for ORL8 cells and T for OR6 cells] located 20 bases upstream from the initiation codon. Luciferase reporter assay using ORL8c cells revealed that the promoter activity of OR6 origin was almost equal to that of ORL8 origin (Supporting Fig. 4A), indicating that the detected SNP was not involved in the level of promoter activity.

We next evaluated the epigenetic effects on ADK expression level. The results revealed that the expression level of ADK mRNA in OR6 cells was not enhanced in the cells treated with 5azaC and/or 4-PBA for 48 hours (Supporting Fig. 4B). Moreover, the protein level of ADK was not increased in the OR6 cells treated with 5azaC for 6 days (Supporting Fig. 4C). Taken together, these results suggest that the low level of ADK mRNA in OR6 cells was not the result of genetic polymorphisms or epigenetic alternations in the ADK gene promoter region.

The Differential ADK Expression Between OR6 and ORL8 Cells Was Not Mediated by a microRNA Control Mechanism. To explain the above-described gap between the 4.5-fold difference in the mRNA level and the 16-fold difference in the protein level (Fig. 1C,E), we hypothesized that the 3' UTR of ADK mRNA was different in the length or nt sequences between OR6 and ORL8 cells, and that such differences affected the control mechanism by microRNA (miRNA). To test this hypothesis, we first performed 3' rapid amplification of cDNA ends (RACE) analysis on ADK mRNA using total RNA prepared from OR6 or ORL8 cells. Sequence analysis using more than 45 cDNA clones obtained from each cell line was carried out. 3' UTRs of four different lengths were detected in both OR6 and ORL8 cells, because four potential poly(A) additional signals were present in the downstream ADK open reading frame (ORF) (Supporting Fig. 5). The results revealed no qualitative difference of 3' UTR species between OR6 and ORL8 cells (Supporting Fig. 5).

Because the 3' UTR of ADK mRNA contained the seed sequences of miR-182, miR-203, mir-125a-3p, and miR-106b (Supporting Fig. 5), we assumed that

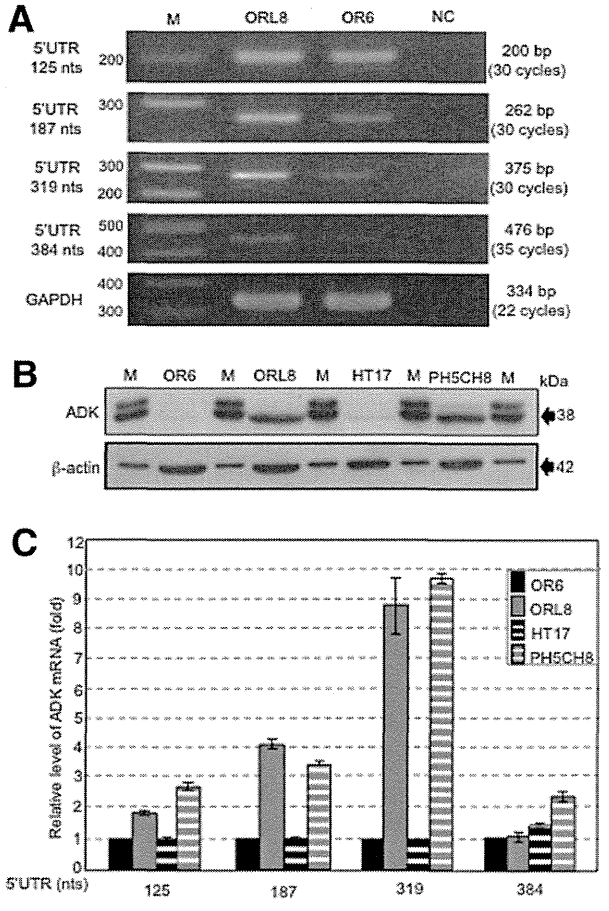

Fig. 3. Level of ADK mRNA possessing long 5' UTR was correlated with the expression level of ADK. (A) Total RNAs prepared from ORL8 and OR6 cells were subjected to RT-PCR using the primer sets (Supporting Table 1) for various lengths of 5' UTR of ADK mRNA. (B) Expression levels of ADK were compared by western blotting analysis. The two molecular markers of ADK shown in Fig. 1E were loaded on every two lanes. (C) Amounts of 5' UTR species of ADK mRNAs were compared by quantitative RT-PCR analysis using the primer sets described in (A). Experiments were performed in triplicate.

the difference in expression levels of these miRNAs causes the different protein levels of ADK. To examine this possibility, we performed an miRNA microarray analysis between OR6 and ORL8 cells. This analysis revealed very low expression levels (measured values of less than 7) of miR-182, miR203, and miR-125a-3p in both cell lines. Although only miR-106b was moderately expressed (measured value of approximately 300) in OR6 and ORL8 cells, the values obtained from both cell lines were almost the same. From these results, these miRNAs may not participate in the translational regulation of ADK mRNAs in OR6 and ORL8 cells.

The 5' UTR of ADK mRNA in ORL8 Cells Was Longer Than That in OR6 Cells. To explain the dramatic difference in ADK expression between ORL8 and OR6 cells, we next focused on the 5' UTR. To date, two different lengths of 5' UTR (384 nts in accession number NM_001123[25-MAR-2011] and 187 nts in accession numbers NM_001123[31-OCT-2010] and HSU_50196) have been deposited in GeneBank. Because the 384 nts form has been considered to be a unique species in testis tissue, we performed 5' RACE analysis to determine the length of the 5' UTR of ADK mRNA in ORL8 or OR6 cells. Sequence analysis was carried out using more than 20 cDNA clones obtained from each cell line. Consequently, we obtained 319 and 125 nts as the major 5' UTR species in ORL8 and OR6 cells, respectively. We confirmed these results by RT-PCR analysis using four different primer sets for the 5' UTR (Fig. 3A). The amount of 384 nts species in ORL8 cells was estimated to be less than one thirtieth the amount of the 319-nts species (Fig. 3A). These results indicate that the length of 5' UTR in ORL8 cells is longer than that in OR6 cells.

From these results, we considered the possibility that the length of the 5' UTR is associated with the protein level of ADK. To test this possibility, we first compared the expression levels of ADK in various human hepatoma cell lines and human immortalized hepatocyte lines. Low expression level of ADK was observed in HT17 and Hep3B cells as well as OR6 cells, although the other cell lines, including ORL8, HuH-6, HepG2, HLE, and PH5CH8 cells, showed high expression level of ADK (Fig. 3B and Supporting Fig. 6). We next performed quantitative RT-PCR analysis on the 5' UTR using total RNAs from OR6, ORL8, HT17, and PH5CH8 cells. Consequently, we found that the 319 nts species of the 5' UTR was abundant in PH5CH8 cells, but not in HT17 cells (Fig. 3C), indicating good correlation between the amount of 319 nts species and the amount of ADK protein (Fig. 3B,C). These results suggest that the 319 nts species of 5' UTR is involved in the high protein level of ADK.

The Long-Form 5' UTR of ADK mRNA Possessed IRES Activity. From the results of 5' UTR analysis, we assumed that the 319 nts species of the 5' UTR possesses IRES activity because it is GC rich (72%) and highly structured (estimated $\Delta G = -110.7$ kcal/mol), and because it contains an upstream ORF for 70 amino acids. To test this assumption, we used a bicistronic dual luciferase reporter assay system for the detection of IRES activity (Fig. 4A). As a positive control, we constructed a pGL4-based reporter plasmid containing HCV IRES (377 nts; 341 nts in the 5' UTR plus the first 36 nts in the Core-encoding

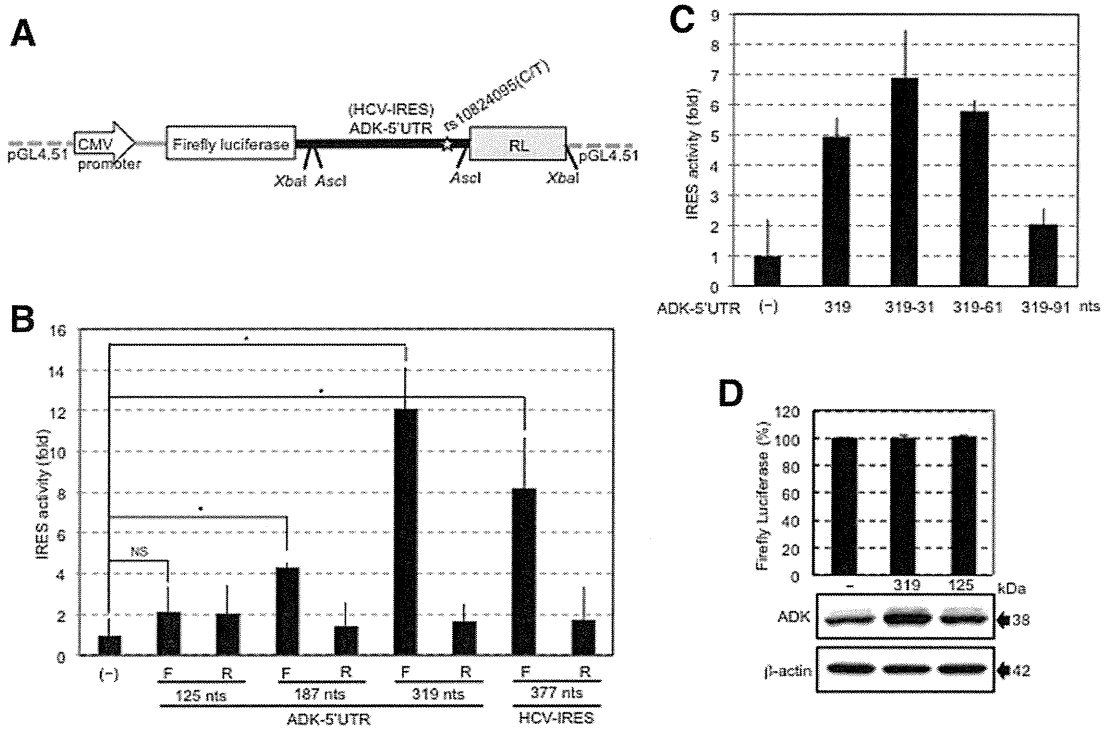

Fig. 4. Long-form 5' UTR of ADK mRNA possessed IRES activity. (A) Partial structure of the plasmid used as a dicistronic dual reporter assay system. (B) ORL8c cells were transfected with the plasmid as shown in (A). After 48 hours, a dual luciferase assay was performed. The ratio of the RL activity to firefly luciferase activity was calculated. The relative value calculated at each sample, when the ratio in the control vector-transfected cells (−) was assigned to be 1, is presented. F and R indicate the forward and reverse direction of insert in the reporter plasmid, respectively. (C) Deletion mutant analysis of the 5' UTR in IRES assay. IRES assay was performed using ORL8c cells transfected with the reporter plasmid containing the deleted forms of the 5' UTR, as described in (B). (D) ADK expression derived from the long-form 5' UTR transcript was more productive than that from the short-form 5' UTR transcript. OR6c cells were transfected with the plasmid, in which the *XbaI* fragment of the plasmid used for HCV IRES activity assay was replaced by the ADK ORF possessing the 5' UTR of 319 or 125 nts. After 48 hours, western blotting analysis was performed. Firefly luciferase activities were measured to check equal transfection efficiency. Experiments (B and C) were performed in triplicate. $*P < 0.05$; NS, not significant.

region). We next replaced the HCV IRES structure in this plasmid with several different lengths (forward or reverse direction) of the 5' UTR derived from ORL8 cells. ORL8c cells were transfected with these plasmids, and at 48 hours after transfection, dual luciferase assays were performed. Consequently, we found that the forward 319 nts, but not the forward 125 nts, of 5' UTR clearly showed IRES activity at the same level as HCV IRES (Fig. 4B). The 187 nts species also showed weak IRES activity (Fig. 4B). None of the 5' UTR species with reverse direction and none of the HCV IRES with reverse direction showed any IRES activities (Fig. 4B). Furthermore, similar results were obtained in the genome-length HCV RNA-replicating OL8 cells and their cured cells (OL8c) (Supporting Fig. 7A,B), suggesting that IRES activity does not depend on cell strains or HCV RNA replication. In addition, we did not observe any effects of an SNP (rs10824095), which was located 20 bases upstream from the initiation codon, on the IRES activities of OR6 and ORL8 cell-derived 5' UTRs (319 nts) (Supporting Fig. 8).

To identify the entry site of the 40S ribosome in the IRES region, we prepared three deletion mutants (deleted upstream 30, 60, and 90 nts from the initiation codon) of the 5' UTR and measured their IRES activities in ORL8c cells. The results revealed that the deletion up to 60 nts from the initiation codon did not decrease IRES activity, but the 90 nts deletion abolished IRES activity (Fig. 4C). Similar results were also obtained in OL8 and OL8c cells (Supporting Fig. 7C,D). These results suggest that the entry site of the 40S ribosome is between 60 and 90 nts upstream from the initiation codon, and that the region from 319 to 61 nts upstream from the initiation codon is necessary for the IRES activity. It is noteworthy that this region forms a stable secondary structure (estimated $\Delta G = -108.4$ kcal/mol) (Supporting Fig. 7E). Furthermore, we demonstrated that ADK expression derived from the long-form 5' UTR transcript was

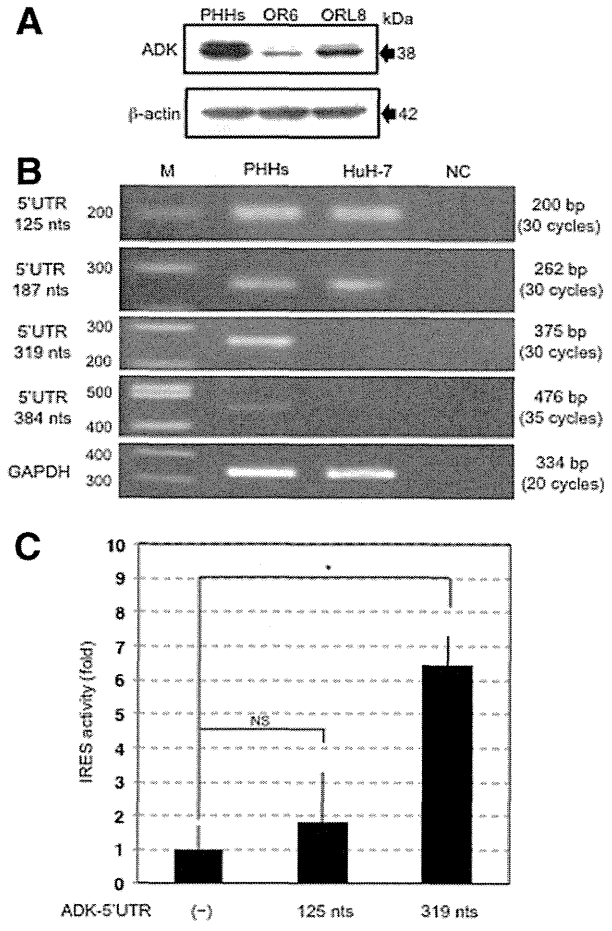

Fig. 5. Long-form 5' UTR of ADK mRNA functioned as an IRES in PHHs. (A) ADK expression level in PHHs was compared with those in OR6 and ORL8 cells by western blotting analysis. (B) Total RNAs prepared from PHHs and HuH-7 cells were subjected to RT-PCR analysis using the primer sets described in Fig. 3A. (C) PHHs were transfected with the plasmid shown in Fig. 4A. After 48 hours, a dual luciferase assay was performed as described in Fig. 4B. Experiments (B and C) were performed in triplicate. $*P < 0.05$; NS, not significant.

more productive than the expression from the short-form 5' UTR transcript in OR6c cells (Fig. 4D).

The Long-Form 5' UTR of ADK mRNA Functioned as an IRES in Primary Human Hepatocytes. To obtain a final conclusion, we examined whether the novel mechanism in ADK translation plays a role in PHHs. We first examined ADK expression level in PHHs, and the results revealed that ADK protein level was higher in PHHs than in ORL8 cells (Fig. 5A). We next performed RT-PCR analysis using the primer sets used in Fig. 3A to examine the amounts of 319 and 125 nts forms of the 5' UTR. The results showed that the 319 nts species was the major 5' UTR species in PHHs, but not in HuH-7 cells, which are the parent of OR6 cells (Fig. 5B), indicating a good correlation between the amount of 319 nts species and the amount of ADK protein in PHHs. Finally, we demonstrated that the 319 nts form, but not the 125 nts form, of 5' UTR clearly showed IRES activity in PHHs (Fig. 5C).

Considering all these results together, we conclude that not only ORL8 cells, but also PHHs express the long-form 5' UTR of ADK mRNA possessing IRES activity and then produce high levels of ADK, which works as an RBV kinase.

Discussion

In this study, we identified, for the first time, a host factor ADK whose expression level could control the anti-HCV activity of RBV. Furthermore, we found that the expression level of ADK was associated with the amount of ADK mRNA possessing long 5' UTR exhibiting IRES activity. This finding suggests that the RBV sensitivity on HCV RNA replication is regulated by the IRES-dependent translation of ADK mRNA. If ADK expression levels or activity differ between patients with CHC, it may be a useful therapeutic target.

It has recently been reported that a functional SNP (rs1127354; major C and minor A) in inosine triphosphatase was the most significant SNP associated with RBV-induced anemia.[18] In this context, we hypothesized that this SNP is associated with the expression level of ADK. To test this hypothesis, we examined the status of rs1127354 in ORL8 and PH5CH8 cells showing high expression levels of ADK and in OR6 and Hep3B cells showing low expression levels of ADK. The results revealed that all cell lines showed the major C of the SNP, suggesting that rs1127354 is not associated with the expression level of ADK.

The most striking highlight in this study is the IRES activity found in ADK mRNA. It has recently been reported that cellular IRES-mediated translation is activated by many physiological and pathological stress conditions in eukaryotic cells.[19] To achieve efficient IRES-dependent translation, some triggers will be needed. However, HCV RNA replication was not such a trigger, in the present study, because a similar level of IRES activity was observed in both OL8c cured cells and genome-length HCV RNA-replicating OL8 cells (Supporting Fig. 7A-D). The addition of adenosine did not act as a trigger for IRES (Supporting Fig. 9). Another possible explanation for the high level of ADK in ORL8 cells would be the involvement of one or more miRNA(s) in stabilizing the IRES-containing ADK mRNA, as reported in HCV RNA.[20] To test this possibility, we performed comparative miRNA microarray analysis using ORL8, PH5CH8, OR6, and HT17 cells. The results revealed that nts 1-8 of miR-

424, whose expression levels in ORL8 and PH5CH8 cells were several times higher than those in OR6 and HT17 cells, showed base pairs in the nt 61-68 upstream initiation codon of ADK mRNA. It was noticed that this region in ADK mRNA overlaps the region (nt 60-90 upstream initiation codon of ADK mRNA) identified as the entry site of the 40S ribosome. However, a preliminary experiment showed that overexpression of miR-424 in ORL8 or OR6 cells did not enhance the translation of ADK (Supporting Fig. 10), suggesting that miR-424 is not associated with the high level of ADK in ORL8 cells. The possibility remains that other miRNA(s) participate in the up-regulation of ADK.

At this time, we have identified ADK as a host factor that controls the anti-HCV activity of RBV and clarified the molecular mechanism underlying regulation with ADK. Furthermore, we demonstrated that such a novel mechanism plays a role in PHHs. From our finding, we suggest that ADK expression is artfully regulated both at the transcription and translation stage. Although we identified ADK, which participates in nucleotidic metabolism, as an enzyme functionally controlled by the specific expression of an IRES-containing mRNA, there may be other gene products controlled by a similar mechanism.

Acknowledgments: The authors thank Naoko Kawahara, Takashi Nakamura, and Keiko Takeshita for their technical assistance.

References

1. Lindenbach BD, Rice CM. Unravelling hepatitis C virus replication from genome to function. Nature 2005;436:933-893.
2. Ghany MG, Nelson DR, Strader DB, Thomas DL, Seeff LB. An update on treatment of genotype 1 chronic hepatitis C virus infection: 2011 practice guideline by the American Association for the Study of Liver Diseases. HEPATOLOGY 2011;54:1433-1444.
3. Jacobson IM, McHutchison JG, Dusheiko G, Di Bisceglie AM, Reddy KR, Bzowej NH, et al. Telaprevir for previously untreated chronic hepatitis C virus infection. N Engl J Med 2011;364:2405-2416.
4. Poordad F, McCone J, Jr., Bacon BR Bruno S, Manns MP, Sulkowski MS, et al. Boceprevir for untreated chronic HCV genotype 1 infection. N Engl J Med 2011;364:1195-1206.
5. Feld JJ, Hoofnagle JH. Mechanism of action of interferon and ribavirin in treatment of hepatitis C. Nature 2005;436:967-972.
6. Paeshuyse J, Dallmeier K, Neyts J. Ribavirin for the treatment of chronic hepatitis C virus infection: a review of the proposed mechanisms of action. Curr Opin Virol 2011;1:590-598.
7. Thomas E, Feld JJ, Li Q, Hu Z, Fried MW, Liang TJ. Ribavirin potentiates interferon action by augmenting interferon-stimulated gene induction in hepatitis C virus cell culture models. HEPATOLOGY 2011;53:32-41.
8. Zhou S, Liu R, Baroudy BM, Malcolm BA, Reyes GR. The effect of ribavirin and IMPDH inhibitors on hepatitis C virus subgenomic replicon RNA. Virology 2003;310:333-342.
9. Ikeda M, Abe K, Dansako H, Nakamura T, Naka K, Kato N. Efficient replication of a full-length hepatitis C virus genome, strain O, in cell culture, and development of a luciferase reporter system. Biochem Biophys Res Commun 2005;329:1350-1359.
10. Mori K, Ikeda M, Ariumi Y, Dansako H, Wakita T, Kato N. Mechanism of action of ribavirin in a novel hepatitis C virus replication cell system. Virus Res 2011;157:61-70.
11. Kato N, Mori K, Abe K, Dansako H, Kuroki M, Ariumi Y, et al. Efficient replication systems for hepatitis C virus using a new human hepatoma cell line. Virus Res 2009;146:41-50.
12. Mori K, Ikeda M, Ariumi Y, Kato N. Gene expression profile of Li23, a new human hepatoma cell line that enables robust hepatitis C virus replication: comparison with HuH-7 and other hepatic cell lines. Hepatol Res 2010;40:1248-1253.
13. Kato N, Sugiyama K, Namba K, Dansako H, Nakamura T, Takami M, et al. Establishment of a hepatitis C virus subgenomic replicon derived from human hepatocytes infected in vitro. Biochem Biophys Res Commun 2003;306:756-766.
14. Dansako H, Naganuma A, Nakamura T, Ikeda F, Nozaki A, Kato N. Differential activation of interferon-inducible genes by hepatitis C virus core protein mediated by interferon stimulated response element. Virus Res 2003;97:17-30.
15. Takatori S, Kanda H, Takenaka K, Wataya Y, Matsuda A, Fukushima M, et al. Antitumor mechanisms and metabolism of the novel antitumor nucleoside analogues, 1-(3-C-ethynyl-beta-D-ribo-pentofuranosyl)-cytosine and 1-(3-C-ethynyl-beta-D-ribo-pentofuranosyl)uracil. Cancer Chemother Pharmacol 1999;44:97-104.
16. Streeter DG, Witkowski JT, Khare GP, Sidwell RW, Bauer RJ, Robins RK, Simon LN. Mechanism of action of 1-β-D-ribofuranosyl-1,2,4-triazole-3-carboxamide (Virazole), a new broad-spectrum antiviral agent. Proc Natl Acad Sci U S A 1973;70:1174-1178.
17. Cui XA, Singh B, Park J, Gupta RS. Subcellular localization of adenosine kinase in mammalian cells: the long isoform of AdK is localized in the nucleus. Biochem Biophys Res Commun 2009;388:46-50.
18. Fellay J, Thompson AJ, Ge D, Gumbs CE, Urban TJ, Shianna KV, et al. ITPA gene variants protect against anaemia in patients treated for chronic hepatitis C. Nature 2010;464:405-408.
19. Komar AA, Hatzoglou M. Cellular IRES-mediated translation: the war of ITAFs in pathophysiological states. Cell Cycle 2011;10:229-240.
20. Shimakami T, Yamane D, Jangra RK, Kempf BJ, Spaniel C, Barton DJ, Lemon SM. Stabilization of hepatitis C virus RNA by an Ago2-miR-122 complex. Proc Natl Acad Sci U S A 2012;109:941-946.

Hepatitis C virus NS4B targets lipid droplets through hydrophobic residues in the amphipathic helices[S]

Torahiko Tanaka,[1,*] Kazumichi Kuroda,[†] Masanori Ikeda,[§] Takaji Wakita,[**] Nobuyuki Kato,[§] and Makoto Makishima[*]

Division of Biochemistry, Department of Biomedical Sciences* and Division of Microbiology, Department of Pathology and Microbiology,[†] Nihon University School of Medicine, Tokyo 173-8610, Japan; Department of Tumor Virology,[§] Okayama University Graduate School of Medicine, Dentistry, and Pharmaceutical Sciences, Okayama 700-8558, Japan; and Department of Virology II,** National Institute of Infectious Diseases, Tokyo 162-8649, Japan

Abstract Lipid droplets (LD) are dynamic storage organelles that are involved in lipid homeostasis. Hepatitis C virus (HCV) is closely associated with LDs. HCV Core and nonstructural (NS) proteins colocalize with LDs and presumably are involved in virion formation at that site. We demonstrated that HCV NS4B, an integral membrane protein in endoplasmic reticulum (ER), strongly targeted LDs. Confocal imaging studies showed that NS4B localized at the margins of LDs. Biochemical fractionation of HCV-replicating cells suggested that NS4B existed in membranes associated with LDs rather than on the LD surface membrane itself. The N- and C-terminal cytosolic domains of NS4B showed targeting of LDs, with the former being much stronger. In both domains, activity was present in the region containing an amphipathic α-helix, in which 10 hydrophobic residues were identified as putative determinants for targeting LDs. JFH1 mutants with alanine substitutions for the hydrophobic residues were defective for virus replication. W43A mutant with a single alanine substitution showed loss of association of NS4B with LDs and severely reduced release of infectious virions compared with wild-type JFH1. NS4B plays a crucial role in virus replication at the site of virion formation, namely, the microenvironment associated with LDs.—Tanaka, T., K. Kuroda, M. Ikeda, T. Wakita, N. Kato, and M. Makishima. **Hepatitis C virus NS4B targets lipid droplets through hydrophobic residues in the amphipathic helices.** ***J. Lipid Res.*** **2013.** 54: **881–892.**

Supplementary key words alanine substitution • confocal imaging • JFH1 • RNA transfection

Cellular lipid droplets (LD) are dynamic organelles connecting storage, metabolism, and dynamics of lipids in eukaryotic cells (1–3). LDs consist of core neutral lipids, mainly triglycerides and cholesteryl esters, and the surrounding phospholipid monolayer. The lipids stored in LDs are used for various cellular events, such as metabolism as an energy source, membrane synthesis, steroid and eicosanoid synthesis, lipoprotein formation, and protein modification. LDs are thought to be generated from endoplasmic reticulum (ER) and move in a microtubule-dependent, bidirectional manner, interacting with other organelles, such as ER, mitochondria, and peroxisomes.

Recently, a close association between LDs and hepatitis C virus (HCV) was revealed (4). HCV infects about 150 million to 200 million people worldwide, and chronic infection is associated with liver steatosis, cirrhosis, and hepatocellular carcinoma. HCV is a positive- and single-stranded RNA virus with about 9,600 nucleotides of genome (5), which codes 10 HCV proteins: Core, envelope 1 (E1), envelope 2 (E2), p7, nonstructural protein (NS)2, NS3, NS4A, NS4B, NS5A, and NS5B. All of these proteins are essential for replication of HCV. Both the 5′ and 3′ untranslated regions (UTR) of the genome are also essential for viral replication: the 5′ UTR has an internal ribosome entry site (6), and the 3′ UTR contains a highly conserved structure, the 3′ X (7, 8). The infectious viral particles were found to contain the VLDL components, such as triglycerides, cholesterol, and apoB and E, and are therefore called "lipoviroparticles" (9–12). HCV infects cells by utilizing the LDL receptor and scavenger receptor B1 in addition to other receptor molecules, such as CD81, claudin 1, and occludin (13). Through the life cycle of HCV, namely, from viral entry to virion release, cellular lipids

This work was supported by the Strategic Research Base Development Program for Private Universities subsidized by the Ministry of Education, Culture, Sports, Science and Technology, Japan (since 2010); by Nihon University Multidisciplinary Research Grant (2010–2011); and by grants-in-aid for research on hepatitis from the Ministry of Health, Labour, and Welfare of Japan.

Manuscript received 20 March 2012 and in revised form 10 January 2013.

Published, JLR Papers in Press, January 12, 2013
DOI 10.1194/jlr.M026443

Abbreviations: ADRP, adipose differentiation-related protein; EGFP, enhanced green fluorescent protein; ER, endoplasmic reticulum; GST, glutathione S-transferase; HCV, hepatitis C virus; LD, lipid droplet; NS, nonstructural (protein); PNS, post-nuclear supernatant; PVDF, polyvinylidene difluoride; UTR, untranslated region.

[1]To whom correspondence should be addressed.
e-mail: tanaka.torahiko@nihon-u.ac.jp

[S] The online version of this article (available at http://www.jlr.org) contains supplementary data in the form of six figures and four tables.

and lipid metabolism, especially in lipoproteins, play important roles (10–12). HCV modulates cellular lipid metabolism to facilitate its replication: for example, HCV upregulates lipogenesis, resulting in accumulation of triglycerides in the increased mass of LDs. Clinically, liver steatosis is found in about half of chronic HCV patients. Liver steatosis occurs also in transgenic mice harboring the HCV Core protein (14). Inhibition of microsomal triglyceride transfer protein activity and VLDL secretion by HCV protein(s) is also an important mechanism of the lipid accumulation in hepatocytes (11). Several studies have shown that many HCV-derived components, such as Core (15) and NS proteins [NS2 (16), NS3, NS4A, NS4B, NS5A (17), and NS5B] and HCV RNAs, also localize at sites close to LDs (4). Core and NS5A are thought to mediate association of these HCV components with LDs (4); however, the molecular mechanisms by which NS proteins associate with LDs remain unclear. Ultrastructural studies showed accumulation of virion-like structures around LDs (18). Although several cellular and viral proteins localize on the LD membrane, consensus signals for LD targeting are not defined (1). Recent reports have shown that LD-targeting activity resides in amphipathic helices (19–23) or in hydrophobic regions (24–26).

Here, we present evidence that HCV NS4B strongly targets LDs. NS4B is a 261-amino-acid, multifunctional protein consisting of N- and C- terminal cytosolic domains and a central membrane domain harboring at least four transmembrane helices (27). NS4B is an integral membrane protein in ER (28) that can induce alteration of the membrane structure to form a membranous web (29), in which HCV RNA replication is thought to occur (30–32). We provide evidence to suggest how ER-resident protein NS4B can interact with LDs. Imaging studies, including a series of mutation analyses, revealed the regions responsible for LD targeting of NS4B. The hydrophobic amino acid residues in amphipathic α-helices are critical for LD targeting. The JFH1 (33) mutant harboring alanine substitutions for the hydrophobic residues of NS4B was defective for virus replication. In a single alanine substitution mutant, W43A, we observed that loss of LD targeting of NS4B caused a severe defect in virus replication. Our results strongly suggest that NS4B functions at sites close to LDs, which is critical for replication of HCV.

MATERIALS AND METHODS

Cell culture system

Oc cells (34) and OR6 HCV-RNA-replicating cells (35) were cultured in collagen (type I)-coated dishes (Iwaki, Chiba, Japan) with DMEM (Sigma) supplemented with 10% FBS, penicillin, and streptomycin.

Antibodies

The antibodies used in this study were those against Core (CP11; MBL, Nagoya, Japan), NS3 (R212), NS4B (52-1, detection for HCV-O NS4B), NS4AB (RR12, detection for JFH1 NS4B), NS5A (8926; BioAcademia, Osaka, Japan), NS5B (NS5B-6, BioAcademia), adipose differentiation-related protein (ADRP; Abcam), FLAG (Sigma), myc-tag (MBL), mCherry (Clontech), glyceraldehyde-3-phosphate dehydrogenase (GAPDH; Millipore), and calnexin (BD Transduction Laboratories). The anti-NS3 (R212), anti-NS4B (52-1), and anti-NS4AB (RR12) antibodies were gifts from Dr. M. Kohara (Tokyo Metropolitan Institute of Medical Science, Japan). Rabbit polyclonal antibodies specific to JFH1 NS3, NS5A, and NS5B were raised against bacterially expressed glutathione S-transferase (GST)-NS3 (amino acids 165–631), GST-NS5A (amino acids 25–466), and GST-NS5B (amino acids 1–570), respectively. Alexa-Fluor-555-conjugated anti-rabbit IgG (Invitrogen), Alexa-Fluor-568-conjugated anti-mouse IgG (Invitrogen), and rhodamine-conjugated anti-mouse IgG (Cappel) antibodies were also used.

Expression plasmids

HCV sequences for expression experiments (NS4B, NS5A and Core) were derived from type 1b HCV strain O [HCV-O, DDBJ/EMBL/GenBank accession number AB191333 (34)]. The HCV fragment was amplified by PCR using the restriction-site-tagged primers with an appropriate template plasmid that contained the desired HCV sequence. To create fusion constructs with fluorescent protein, the *Bgl*II-*Eco*RI-digested PCR fragment was ligated with *Bgl*II-*Eco*RI-digested pmCherry-C1 or pEGFP-C1 vector (Clontech). In another case, the *Nhe*I-*Hin*dIII-digested PCR fragment was ligated with *Nhe*I-*Hin*dIII-digested pcDNA3.1(+) vector (Invitrogen) to create expression constructs. To create a mutant fragment, primers that had desired mutated sequences were used for PCR, and usually two appropriate PCR fragments, namely, "-N" and "-C," were connected by overlapping PCR. Sequences of the primers and their usage, and which fragment the primer sets amplified, are described in supplementary Tables I and II, respectively. pDsRed2-ER, which expressed an ER marker protein, was obtained from Clontech. For construction of enhanced green fluorescent protein (EGFP)-ADRP and Cherry-ADRP, ADRP cDNA was synthesized from Superscript III (Invitrogen) with a primer 5′-CCACAGCATGCACTAGTGAT-3′ from total RNAs prepared from Oc cells with Trizol reagent (Life Technologies) according to the manufacturer's protocol. The ADRP fragment was amplified using the restriction-site-tagged primers 5′-TTTAGATCTATGGCATCCGTTGCAGTTGA-3′ and 5′-TTTGAATTCTTAATGAGTTTTATGCTCAGATCGC-3′, digested with *Bgl*II and *Eco*RI, and ligated with the *Bgl*II-*Eco*RI-digested pmCherry-C1 or pEGFP-C1 vector.

Transient expression experiment

Oc cells (10^5 cells/well) were seeded on a glass-based, 24-well culture plate (EZView, Iwaki), and after being cultured for 16 h, the cells were transfected with expression plasmids with the aid of Lipofectamine 2000 (Invitrogen) according to the manufacturer's protocol. Usually, 1.6 μg plasmid was used for each well with 1:2.5–3 ratio to the lipofection reagent. When two kinds of plasmids were cotransfected into cells, 1.0–1.6 μg of the plasmid was used.

Immunofluorescence

After 24 h transfection, the cells were fixed with 4% paraformaldehyde for 15 min, permeabilized with 0.01% digitonin for 30 min, and stained with Bodipy 493/503 as described previously (36). When antigens were visualized by indirect immunofluorescence, the fixed permeabilized cells were blocked with 1% BSA in TBS (20 mM Tris-HCl, 0.15 M NaCl, pH 7.4) and reacted with an appropriate dilution of primary antibody in 1% BSA-TBS for 1 h at room temperature. After three washes with TBS, the cells were incubated with an Alexa-Fluor-dye-conjugated (Invitrogen) or rhodamine-conjugated (Cappel) secondary antibody with 1,000-fold dilution in 1% BSA-TBS for 30 min. Cell nuclei were stained with Hoechst 33342 for 20 min (nuclei were stained in most of the

experiments but not always shown in the figures). The fluorescent images were collected by confocal laser scanning microscope FV1000 (Olympus, Tokyo, Japan) in a sequential scanning mode.

Immunoblotting

Proteins were resolved on 8 or 12% SDS-PAGE and transferred to polyvinylidene difluoride (PVDF) membranes (GE Healthcare). The membranes were rinsed in water and then soaked in TBS-0.1% Tween 20 (TBST) for 30 min to enhance detection sensitivity (37). The membranes were again rinsed in water and blocked with PVDF Blocking Reagent (Toyobo, Osaka, Japan) for 1 h at room temperature. The membranes were reacted with an appropriate dilution of primary antibody in Can Get Signal Immunoreaction Enhancer Solution 1 (Toyobo) for 1 h at room temperature. After washing with TBST (five times for 10 min each), the membranes were reacted with an appropriate dilution of horseradish-peroxidase-conjugated secondary antibody in Can Get Signal Immunoreaction Enhancer Solution 2 (Toyobo) for 30 min at room temperature. After washing with TBST (five times for 10 min each), the blots were visualized by an ECL Plus immunoblot detection system (GE Healthcare).

Construction of JFH1 mutant

We generated JFH1 (33) (DDBJ/EMBL/GenBank accession number AB047639) mutant constructs that contained alanine substitutions for hydrophobic residues in the NS4B region as follows: 4Bmtmt, W43A, V46A, W50A, F57A, I61A, L64A, I242A, L246A, L249A, and I253A; 4Bmt0, W43A, V46A, W50A, F57A, I61A, and L64A; 4Bmt1, W43A, V46A, and W50A; 4Bmt2, F57A, I61A, and L64A; and 4Bmt3, I242A, L246A, L249A, and I253A. Mutants harboring single alanine substitutions, W43A, V46A and W50A, were also created. To create a mutant fragment, primers with the desired mutated sequences were used for PCR, and two or three appropriate PCR fragments ("-N" and "-C"; or "-N1," "-N2," and "-C") were connected by overlapping PCR. The resultant mutant fragment was digested with *Nsi*I and *Rsr*II and ligated with *Nsi*I-*Rsr*II-digested pJFH1 (33). Sequences of the primers and their usage and which fragment the primer sets amplified are described in supplementary Tables III and IV, respectively.

In vitro transcription and electroporation of viral RNA into Oc cells

pJFH1 and its mutant plasmids were linearized with *Xba*I followed by treatment with mung bean nuclease (Toyobo) according to the manufacturer's protocol. RNA was transcribed in vitro from the linearized constructs using MEGAscript T7 kit (Ambion) and purified with MEGAclear kit (Ambion) according to the instruction manual. RNA integrity was checked by agarose gel electrophoresis. Prior to electroporation, Oc cells were trypsinized and resuspended in complete DMEM. The cells were washed twice with PBS and resuspended in buffer R (Invitrogen) at a concentration of 10^7 cells/ml. JFH1 and mutant RNA was introduced into the Oc cells using the NEON transfection system (Invitrogen) according to the instruction manual as follows. For titration of virus production, 0.5 μg RNA was introduced into 10^5 cells in a 10 μl tip supplied by the manufacturer with two pulses of 30 ms at 1,150 V. Usually, four shots of the electroporated cells (4×10^5 cells) are pooled in 4 ml prewarmed DMEM supplemented with 10% FBS and seeded into 12-well plates (1 ml for each well). For preparation of LDs, 5 μg RNA was introduced into 10^6 cells in a 100 μl tip supplied by the manufacturer, with two pulses of 30 ms at 1,150 V. Three shots of the electroporated cells (3×10^6 cells) were pooled in 30 ml prewarmed DMEM supplemented with 10% FBS and seeded into dishes with a diameter of 10 cm (10 ml each). At 48 h posttransfection, LDs were prepared as described below.

Cell fractionation by step-wise sucrose density gradient

OR6 cells were fractionated in sucrose density gradient as described previously (38) with minor modifications. Twelve hours before preparation, 100 μM oleate was added to the culture medium. Cells (2×10^6 to 3×10^6 cells) were homogenized in 0.5 ml buffer A [10 mM tricine, 3 mM EDTA, and Complete Protease Inhibitor Cocktail (Roche), pH 7.4] containing 0.25 M sucrose with 30 strokes of a glass Dounce homogenizer using a tight-fitting pestle. The lysate was centrifuged for 10 min at 1,000 *g* at 4°C. The sucrose concentration of the postnuclear supernatant (PNS) was adjusted to 26% by adding buffer A containing 60% sucrose. In a 5 ml ultracentrifuge tube (5PA; Hitachi Koki, Tokyo, Japan), 0.34 ml buffer A containing 51% sucrose and 0.75 ml buffer A containing 43% and 35% sucrose were layered. Subsequently, 0.63 ml 26% sucrose-PNS was layered on top of this. Following this, 0.75 ml buffer A containing 18% and 10% sucrose was layered sequentially onto the PNS fraction. Finally, 0.97 ml of buffer A containing 2% sucrose was loaded on top. The step-wise gradient was centrifuged at 32,000 rpm, at 4°C for 90 min using an S52ST rotor (Hitachi Koki). Following centrifugation, the samples (0.5 ml each) were collected from the bottom.

Preparation of LDs

LDs were prepared as described previously (4) with minor modifications. Twelve hours before preparation, 100 μM oleate was added to the culture medium. Samples and buffers were handled on ice or at 4°C through the procedures below. Cells (~3×10^6 OR6 or Oc cells transfected with JFH1 or mutant RNA) were pelleted by centrifugation at 3000 rpm for 5 min at 4°C. The pellet was resuspended in 1.2 ml hypotonic buffer (50 mM HEPES, 1 mM EDTA, 2 mM $MgCl_2$, and Complete Protease Inhibitor Cocktail, pH 7.4) and incubated for 10 min. The suspension was homogenized with 30 strokes of a glass Dounce homogenizer using a tight-fitting pestle, followed by addition of 120 μl 10× sucrose buffer [0.2 M HEPES, 1.2 M potassium acetate, 40 mM $Mg(oAc)_2$, and 50 mM DTT, pH 7.4]. The nuclei were removed by centrifugation at 2,000 rpm for 10 min at 4°C. The supernatant was collected and centrifuged at 16,000 *g* for 10 min at 4°C. The supernatant (S16, 1.25 ml) was mixed with 1.25 ml 1.04 M sucrose in isotonic buffer (50 mM HEPES, 100 mM KCl, 2 mM $MgCl_2$, and Complete Protease Inhibitor Cocktail). The solution was set at the bottom of 5 ml 5PA ultracentrifuge tubes, and 2.5 ml isotonic buffer was loaded onto the sucrose mixture. The gradient was centrifuged at 100,000 *g* in an S52ST rotor for 45 min at 4°C. After centrifugation, the LD fraction on the top of the gradient solution was collected as the first LD fraction (LD1). After 0.1 ml of the fraction was removed for analysis, the volume of the LD1 fraction was then adjusted to 1.25 ml with isotonic buffer and the fraction was mixed with 1.25 ml isotonic buffer containing 1.04 M sucrose. The fraction was set at the bottom of the ultracentrifuge tube and centrifuged again at 100,000 *g* as described above. The LD fraction on the top of the gradient solution was collected as the second LD fraction (LD2).

Titration of HCV infection

Culture supernatant of RNA-transfected cells was filtrated (0.45 μm pore filter) and assayed for infectivity titer by the endpoint dilution method. Before 16 h inoculation, Oc cells were seeded into 96-well plates at a density of 8×10^3/well. Samples were serially diluted 10-fold in complete growth medium, and 20 μl (when necessary, 100 μl) was inoculated into Oc cells in each well in duplicate. After three days of incubation, the cells were

immunostained by anti-Core antibody (CP11). Positive foci were counted, and the infectivity titer was calculated from the average number of foci counted in the last and second-to-last wells of the dilution series that still contained positive foci. The virus titer was expressed as focus-forming units per milliliter of supernatant.

RESULTS

The intrinsic localization of NS4B to LDs

To clarify whether NS4B associated with LDs by itself and the mechanisms of LD targeting by NS4B, we performed fluorescent imaging using confocal microscopy (**Fig. 1** and supplementary Fig. I). NS4B was fused with mCherry or EGFP, and subcellular localization of the fusion proteins was observed simultaneously with that of LDs in Oc cells. LDs were visualized by Bodipy 493/503. We confirmed that the native forms of mCherry or EGFP, found in both cytosol and the nucleus, showed no colocalization with LDs (supplementary Fig. I-A). When the full-length NS4B was fused with the color proteins (Cherry-4B1–261 and EGFP-4B1–262), a major portion of NS4B showed a membranous, reticular pattern of localization in both cases, suggesting the localization to ER. Upon coexpression with an ER marker construct pDsRed2-ER (DsRed-ER), which contained the ER-targeting sequence of calreticulin and the ER retention signal KDEL, localization of NS4B was consistent with that of the ER marker (supplementary Fig. I-A). This suggested that the full-length NS4B resided in ER membrane as previously reported (28, 39). However, we found a small level of ring-shaped localization of NS4B surrounding the green circular fluorescence of Bodipy, which may correspond to the margin of LDs (Fig. 1A and supplementary Fig. I-B). This ring-shape localization pattern merged with that obtained with anti-ADRP antibody (data not shown), suggesting that NS4B localized to the surface of LDs (LD membrane itself or ER membranes associated with LDs). To confirm the colocalization of NS4B with ADRP, we made fusion constructs of ADRP with color fluorescent proteins and coexpressed them with NS4B (Fig. 1B). The fusion constructs of ADRP (Cherry-ADRP and EGFP-ADRP) showed clear ring-shape localization, and the images of Cherry-ADRP and EGFP-ADRP were completely merged, indicating their localization to the LD membranes (Fig. 1B). When Cherry-4B1–261 was coexpressed with EGFP-ADRP, a portion of Cherry-4B1–261 showed ring-shape localization that was consistent with that of EGFP-ADRP, suggesting colocalization of the fusion proteins (Fig. 1B and supplementary Fig. I-C). Thus, a portion of expressed NS4B was thought to localize on the surface of LDs. To represent the degree of LD targeting for each

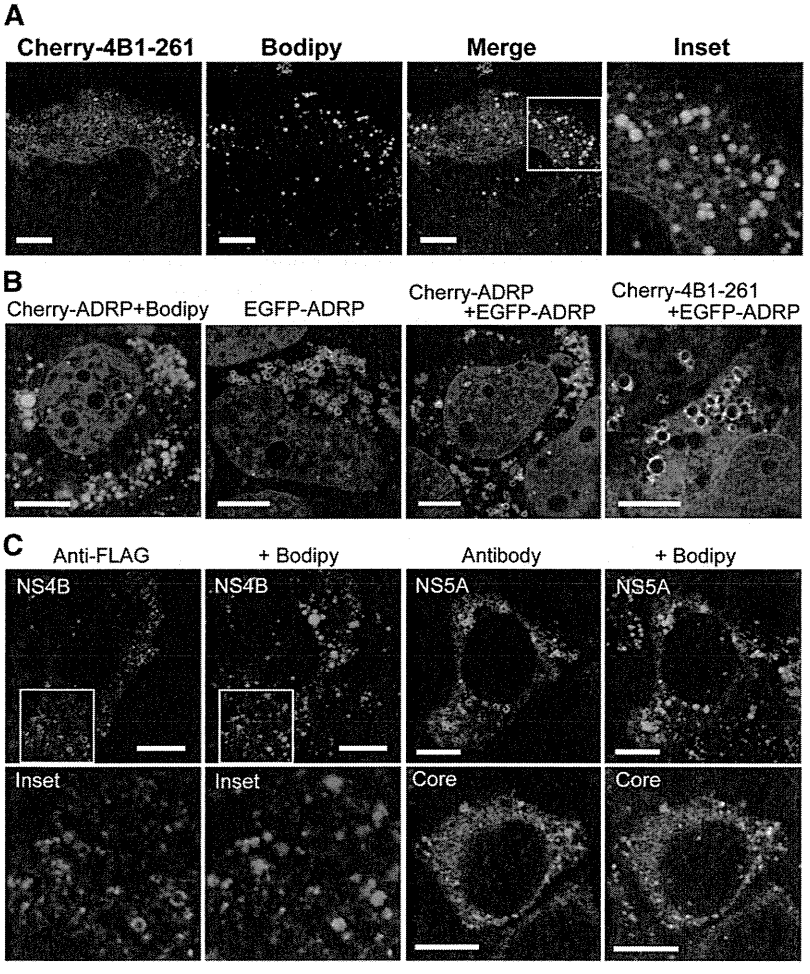

Fig. 1. Full-length NS4B localizes to LDs. (A) Localization of Cherry-4B1–261. Oc cells were transfected with Cherry-4B1–261 for 24 h followed by staining with Bodipy493/503. (A, inset) magnified image. Scale bars, 10 μm. (B) Colocalization of Cherry-4B1–262 with ADRP. From left, Cherry-ADRP, EGFP-ADRP, Cherry-ADRP with EGFP-ADRP (cotransfection), and Cherry-4B1–261 with EGFP-ADRP (cotransfection) was transfected into Oc cells. Scale bars, 10 μm. (C) Localization of NS4B, NS5A, and Core protein. Oc cells were transfected with pcDNA-4B1–261-FLAG (left), pcDNA-5A-myc (right, top), or pcDNA-CORE (right, bottom) for 24 h. After fixation, the antigens were visualized with anti-FLAG (NS4B), anti-Myc (NS5A), or anti-Core antibodies and Alexa-Fluor-dye-labeled secondary antibodies. Scale bars, 10 μm. Inset, magnified image.

construct, we categorized the NS4B-expressing cells (for at least 50 transfectants) into the following four categories: exclusive or dominant localization of the protein to LDs in the observed section (category I); apparent (but not dominant) localization to LDs (category II); slight localization to LDs (with 1–5 rings surrounding LDs seen in the section, category III); and no localization to LDs (category IV). For Cherry-4B1–261 transfectant, about 4 and 15% of the cells were classified into categories I and II, respectively (the results of the count are described in **Table 1**). Thus, NS4B colocalized with LDs in about 20% of cells.

We next expressed full-length NS4B fused with an epitope tag FLAG (amino acid sequence, DYKDDDDK) (pcDNA4B1–261-FLAG) and detected it using an anti-FLAG antibody (this is because we could not obtain antibodies that detected NS4B in HCV-O via immunofluorescence). In most cases, the stain showed differently sized dots, but no clear reticular pattern was obtained. However, we also found that, in some cells, the small dots of NS4B surrounded LDs, suggesting LD localization of FLAG-tagged NS4B (Fig. 1C). Thus, NS4B localizes to LDs by itself. A similar pattern of LD localization was observed for HCV NS5A [tagged with myc (EQKLISEEDL) at the C terminus] and Core, which are known to associate with the LD surface (Fig. 1C). We also found that NS5AΔ1–30, which lacks the N-terminal amphipathic α-helix (amino acids 1–30), did not localize to LDs (data not shown). We conclude that NS4B has an intrinsic activity to target the surface of LDs.

Subcellular distribution of NS4B in OR6 cells

We investigated whether intact NS4B targets LDs in the presence of other HCV proteins. We could not obtain antibodies applicable to immunofluorescent study for HCV-O; therefore, we adopted a biochemical approach. Subcellular fractionation of OR6 HCV-RNA-replicating cells was performed and distribution of HCV antigens was examined by immunoblotting. In OR6 cells, genome-length RNA of HCV-O (fused with *Renilla* luciferase gene for monitoring of HCV genome replication) was stably replicated; hence, intact functional HCV antigens were expressed in the cells. Distributions of cellular and HCV antigens in fractions obtained from OR6 cells by discontinuous sucrose density gradient (38) are shown in **Fig. 2** (left). ADRP was detected most abundantly in the top fraction (fraction 10) followed by fraction 9, suggesting that LDs were enriched in fraction 10 and partly in fraction 9. Calnexin, a marker protein of ER, was found mostly concentrated in fraction 2, showing that a major portion of ER was fractionated into fraction 2. A small portion of calnexin was also enriched in fraction 9 (and 10), suggesting that this fraction contained ER membranes associated with LDs. HCV antigens (Core, NS3, NS4B, NS5A, and NS5B) were detected most abundantly in fraction 2, suggesting that these HCV antigens were associated with ER membranes. However, a small portion of HCV antigens, especially Core, NS4B and NS5A, were clearly detected in fractions 10 and 9. This suggested that a substantial amount of HCV antigens, including NS4B, were present in LD-associated ER membranes or in the LD membrane itself in OR6 cells.

We also prepared LDs from OR6 cells using sucrose density gradient fractionation (by two rounds of discontinuous sucrose gradient ultracentrifugation) as previously described (4) (Fig. 2, right). LD1 was a crude LD preparation after the first ultracentrifugation, and LD2 was the final LD preparation from the second ultracentrifugation. To evaluate the enrichment of antigens to LDs, the amount of each fraction used for immunoblotting was adjusted to give approximately equal signal intensities for ADRP. LD1 seemed to contain a small amount of ER proteins, presumably LD-associated, because a small amount of calnexin was detected in LD1. A small amount of NS4B was detected in LD1 (and a small amount in LD2 with a long chemiluminescence lifetime; data not shown). NS5A was clearly detected in LD1, and a small amount in LD2 as expected. However, Core protein was not detected in either LD preparation, even with longer exposure.

TABLE 1. LD-targeting activity of various NS4B constructs

Construct	Category (% Cells)			
	I	II	III	IV
Cherry-4B1–261[a]	3.7 ± 1.5	15 ± 7	11 ± 4	71 ± 9
Cherry-4B1–73[a]	71 ± 12	29 ± 12	0	0
Cherry-4B74–191	0	0	0	100
Cherry-4B192–261[a]	14 ± 7	34 ± 5	22 ± 9	30 ± 8
Cherry-4B1–49	0	0	0	100
Cherry-4B26–73	15	45	21	19
Cherry-4B1–25	0	0	0	100
Cherry-4B26–49	0	0	0	100
Cherry-4B50–73	0	2	21	77
Cherry-4B192–239	0	0	2	98
Cherry-4B218–261	0	0	10	90
Cherry-4B192–217	0	0	0	100
Cherry-4B218–239	0	0	0	100
Cherry-4B240–261	0	0	8	92
pcDNA-4B1–261-FLAG	0	3	5	93

The degree of LD targeting for each cell is expressed as category I, II, III, or IV. Each construct was transfected into Oc cells, and the percentages of cells with each category are shown.
[a]Results are mean ± SD from three independent experiments.

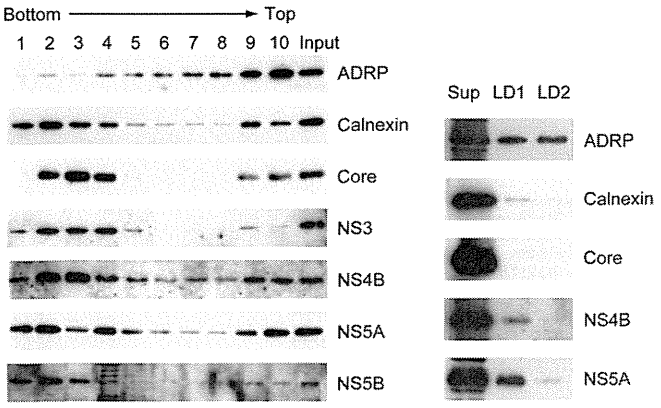

Fig. 2. Localization of HCV antigens to LDs in OR6 cells. (Left) Distribution of cellular and HCV antigens in fractions obtained by discontinuous sucrose density gradient ultracentrifugation (51, 43, 35, 26, 18, 10, and 2% sucrose from bottom to top). OR6 cells were fractionated. The 1/100 vol of each fraction (1–10) and 1/1,000 vol of original PNS (Input) were run on 12% SDS-PAGE followed by immunoblot analysis. (Right) Localization of HCV antigens to LD preparations. LDs were prepared from OR6 cells. LD1, LD preparation obtained from first ultracentrifugation; LD2, final LD preparation obtained from second ultracentrifugation; Sup (S16), supernatant after 16,000 *g* centrifugation. Fractions were analyzed by immunoblotting. The amount of each fraction applied for immunoblotting was adjusted to give approximately equal signal intensity for ADRP. The apparent molecular weights of the indicated proteins were: ADRP, 52 kDa; calnexin, 90 kDa; Core, 21 kDa; NS3, 70 kDa; NS4B, 27 kDa; NS5A, 56/58 kDa; and NS5B, 66 kDa.

NS4B of JFH1 strain targets LDs in RNA-transfected cells

HCV strain JFH1 (subtype 2a) is the first effective replication/infection system of HCV (33). When the genome-length JFH1 RNA is transfected into HuH-7 and its derivative cells, virus replication occurs in cells and infectious virion is released into the culture medium. We transfected JFH1 RNA into Oc cells and prepared and analyzed the LDs by immunoblotting (supplementary Fig. II). NS3, NS4B, NS5A, and NS5B proteins were all positive in both LD1 and LD2. NS4B was apparently enriched in LD1 as compared with the ratio of calnexin content between Sup (S16) and LD1, but it was much less abundant in LD2 than in LD1. This distribution profile suggested that NS4B was localized to LD-associated ER membranes rather than to the LD membranes themselves. Core protein was not detected in LD preparations as in those of OR6 cells; instead, it was precipitated to the bottom of the ultracentrifugation tube.

NS4B has two independent LD-targeting regions in the N- and C-terminal cytosolic domains

To determine which regions or motifs in NS4B were responsible for the targeting to LDs, various NS4B constructs of HCV-O were prepared as fusion proteins with mCherry (**Fig. 3A**). The results were similar for mCherry and EGFP constructs; therefore, we chose mCherry as a tag protein together with Bodipy 493/503 to stain LDs. We determined the activity of the N- and C-terminal cytosolic domains and the central membrane domain (Fig. 3B and Table 1). Crystal structure analysis is not yet possible for NS4B; therefore, the boundary of the N-terminal and central membrane domains was not determined. The boundary of the central and C-terminal domains has been determined from the secondary structure prediction as being between 191 and 192 (27). We tentatively defined the domains as amino acids 1–73, 74–191, and 192–261, respectively, and expressed them in Oc cells. We found that the N-terminal domain (Cherry-4B1–73) showed a strong LD localization. For Cherry-4B1–73, about 70% of the cells were counted as category I and 30% as II; therefore, in nearly all of the cells, the N-terminal domain of NS4B showed LD localization. When the membrane domain (Cherry-4B74–191) was expressed in cells, many ring-shaped localizations were seen, but they had no relation with LDs (Fig. 3B). This ring-shape structure implies that NS4B activity can alter the membrane structure of ER, forming a "membranous web" (29).

The C-terminal domain (Cherry-4B192–261) also showed LD localization, but to a lesser extent than that of the N-terminal region: ~10% of the cells were category I, and 30% were category II. To identify the detailed LD-binding region, each terminal region was further divided into three, and their localization or that of the region spanning the two parts (two thirds of the terminal domain) was determined (Fig. 3C, D and Table 1). For the N-terminal region, Cherry-4B26–73 showed significant LD targeting. Within the amino acid residues 26–73, Cherry-4B26–49 showed no activity, whereas Cherry-4B50–73 was slightly active. Although the degree of localization was much lower than that of Cherry-4B1–73, the N-terminal site for LD localization was identified in the C-terminal half (or one third) of the N-terminal domain (Table 1). Regarding the C-terminal region, Cherry-4B218–261 and Cherry-4B240–261 were slightly active, suggesting that the C-terminal site is in the C-terminal half (or one third) of the C-terminal domain, although the region had little activity by itself (Table 1). Thus, NS4B had two independent regions for targeting LDs.

Hydrophobic amino acid residues in amphipathic α-helices in NS4B are critical for LD targeting

For both the N- and C-terminal sites, an amphipathic α-helix has been identified: amino acids 40–69 for the N-terminal region, and 229–253 for the C-terminal region. Both helices are thought to mediate membrane association of NS4B (40, 41). Amphipathic helices are also known to mediate LD association (19–23); therefore, we hypothesized that the amphipathic helices, especially the hydrophobic amino acids within them, were important for LD targeting of NS4B. From helical wheel projection analysis (http://rzlab.ucr.edu/scripts/wheel/wheel.cgi, provided by D. Armstrong et al.), we noticed that 10 hydrophobic residues (43W, 46L, 50W, 57F, 61I, and 64L for the N-terminal amphipathic helix; 242I, 246L, 249L, and 253I for the C-terminal amphipathic helix) were present on the hydrophobic faces of the helices (**Fig. 4**). To establish whether these residues were involved in LD targeting, we made various alanine substitutions for the residues. The influence of mutations was evaluated by reduction of LD localization as compared with the mother constructs (Fig. 4).

When all of the six residues in the N-terminal amphipathic helix were substituted by alanine (Cherry-4B1–73mt1), the

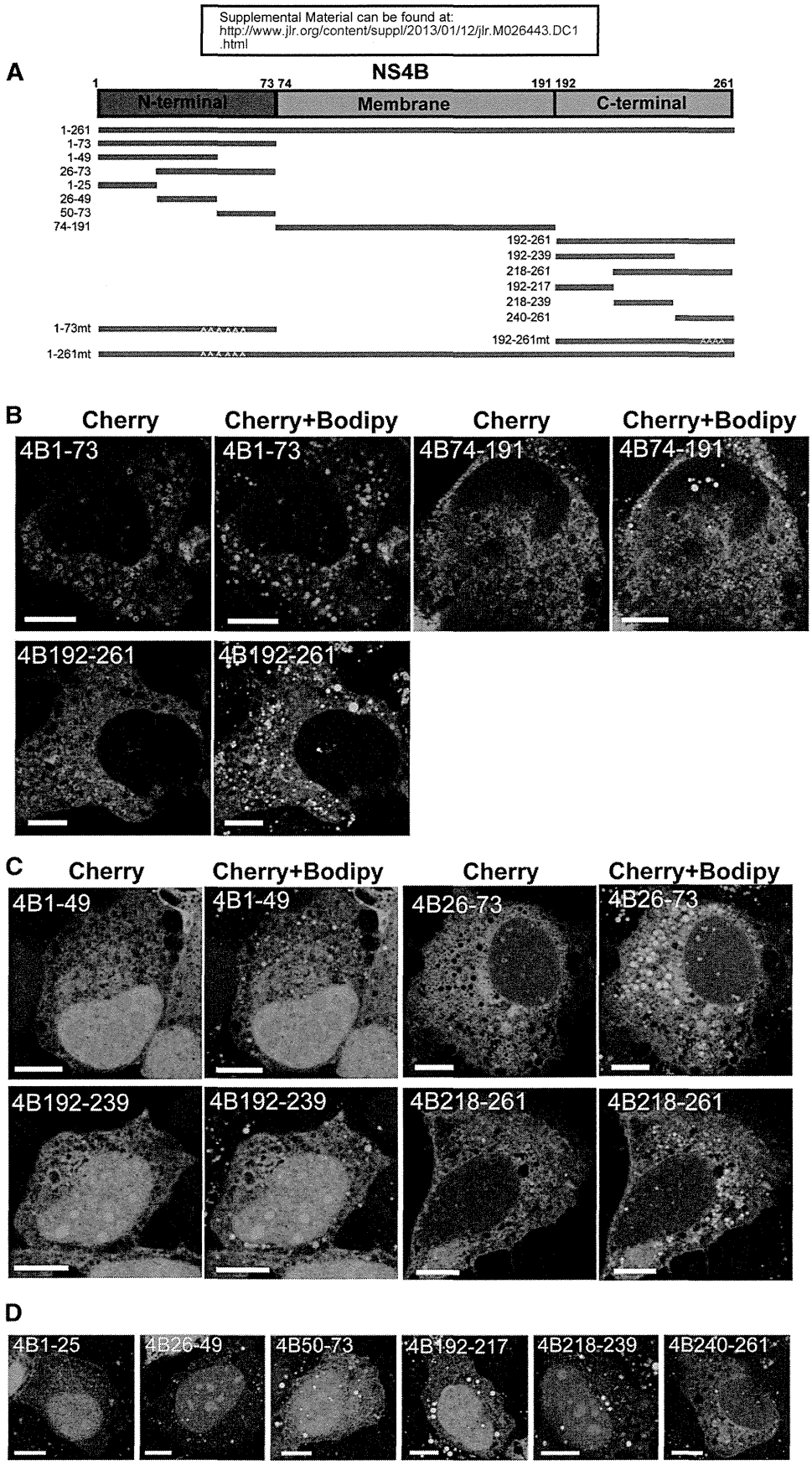

Fig. 3. Two independent target sites for LDs are present in NS4B. (A) Schematic representation of the intact and mutant NS4B. NS4B proteins were N-terminally tagged with mCherry protein. Numbers indicate the amino acid position in NS4B, and mt denotes the alanine substitution construct. (B) Localization of the N-terminal, central, and C-terminal domains of NS4B. Oc cells were transfected with Cherry-4B1–73, Cherry-4B74–191, or Cherry-4B192–261 for 24 h, and then fixed and stained with Bodipy 493/503. (C, D) Localization of the subdivided N- and C-terminal domains of NS4B. (B–D) Scale bars, 10 μm.

Supplemental Material can be found at:
http://www.jlr.org/content/suppl/2013/01/12/jlr.M026443.DC1.html

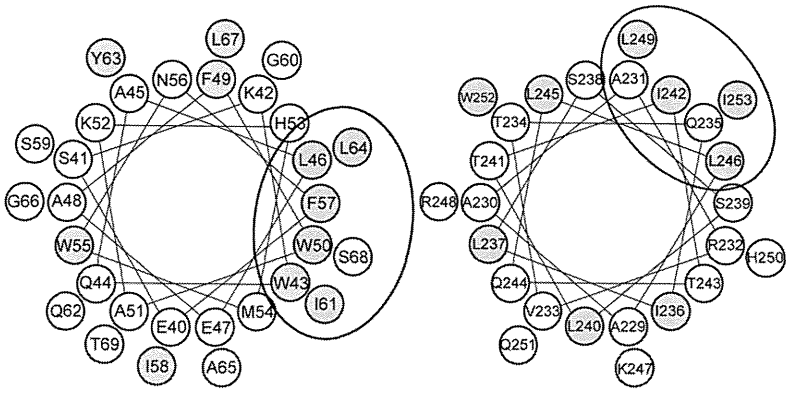

	Degree of LD targeting (Category)			
	I	II	III	IV
	(% cells)			
Cherry-4B1-73mt1 (W43A, L46A, W50A, F57A, I61A, L64A)	0	0	0	100
Cherry-4B1-73mt2 (W43A, L46A, W50A)	0	24	25	51
Cherry-4B1-73mt3 (F57A, I61A, L64A)	27	61	11	2
Cherry-4B1-73mt4 (W43A)	51	49	0	0
Cherry-4B1-73mt5 (L46A)	61	39	0	0
Cherry-4B1-73mt6 (W50A)	68	30	2	0
Cherry-4B192-261mt1 (I242A, L246A, L249A, I253A)	0	0	2	98
Cherry-4B1-261mt1 (W43A, L46A, W50A, F57A, I61A, L64A)	0	0	5	95

Fig. 4. Hydrophobic amino acid residues in amphipathic α-helices are critical for targeting LDs. (Top) Helical wheel projection analysis (http://rzlab.ucr.edu/scripts/wheel/wheel.cgi) for amphipathic α-helices in the N-terminal (left) and C-terminal (right) domains. Hydrophobic residues (W, F, Y, L, I) are shown as gray circles. The ellipse shows a putative hydrophobic face. (Bottom) Inhibition of LD-targeting activity by alanine substitutions for the hydrophobic residues. Localization to LDs was determined for each mutant, and the degree of LD targeting is presented by the percentages of cells classified into categories I–IV. Category I, expressed protein localized to LDs exclusively or dominantly; category II, expressed protein localized to LDs apparently but not dominantly (at least six ring-shape localizations surrounding LDs are seen in the section); category III, expressed protein slightly localized to LDs (1–5 ring-shape localizations surrounding LDs are seen in the section); category IV, expressed protein did not localize to LDs.

LD-targeting activity of Cherry-4B1–73 completely disappeared. As a result of a six-residue interval between 50W and 57F, the hydrophobic residues could be segregated into two clusters of three hydrophobic residues each. When the three residues of the cluster were substituted simultaneously, the influence on the LD-targeting activity was stronger by mutating the upstream cluster (Cherry-4B1–73mt2, containing W43A, L46A, and W50A) than the downstream cluster (Cherry-4B1–73mt3, containing F57A, I61A, and L64A) (Fig. 4). The single residue substitution in the upstream cluster, W43A, L46A, or W50A, did not significantly affect the LD-targeting activity of Cherry-4B1–73 (Cherry-4B1–73mt4, mt5, and mt6). The results indicated that the hydrophobic residues in the amphipathic helix were required for the LD-targeting activity in the N-terminal domain of NS4B, in which the residues in the upstream cluster (43W, 46L, and 50W) had a relatively stronger effect in a synergistic manner.

Regarding the C-terminal domain of NS4B, we made alanine substitutions for all four residues simultaneously (Cherry-4B192–261mt1, containing I242A, L246A, L249A, and I253A), because the activity of the mother Cherry-4B192–261 was relatively low (Table 1). This mutant showed no activity for LD targeting. Although the degree of contribution from each residue was not clear, these hydrophobic amino acids were considered to be critical for the LD-targeting activity of the C-terminal domain. Similarly, we made six alanine substitutions simultaneously (W43A, L46A, W50A, F57A, I61A, and L64A) in a full-length NS4B construct (Cherry-4B1–261mt1), because of the relatively low targeting activity of the mother construct Cherry-4B1–261. This alanine mutant showed no apparent activity for LD targeting, indicating that the hydrophobic residues were critical for LD targeting of full-length NS4B.

When the expression of cherry fusion proteins was checked by immunoblotting, each construct showed its predicted molecular weight, although differences in expression level were seen among the different constructs (supplementary Fig. III). Cherry-4B1–73 and its mutants showed dual bands by unknown mechanisms; however, this seemed to be unrelated to the degree of LD-targeting for each protein. It should be noted that the 10 amino acid residues described here (43W, 46L, 50W, 57F, 61I, 64L, 242I, 246L, 249L, and 253I) were highly conserved among the wide variety of subtypes of HCV, supporting their critical role in the virus life cycle (supplementary Fig. IV).

JFH1 mutants harboring alanine substitutions abolishing LD-targeting activity of NS4B are defective for replication

To clarify the importance of LD targeting of NS4B for replication of HCV, we examined JFH1 mutants that contained alanine substitutions of hydrophobic residues critical for LD targeting in the NS4B region. The 10 hydrophobic residues, 43W, 46V (L in strain O), 50W, 57F, 61I, 64L, 242I, 246L, 249L, and 253I, were divided into three clusters as described above, and mutants were created for each cluster of three or four simultaneous alanine substitutions: 4Bmt1, W43A, V46A, and W50A; 4Bmt2, F57A, I61A, and L64A; and 4Bmt3, I242A, L246A, L249A, and I253A. When the wild-type and mutant RNAs were transfected into Oc cells, wild-type JFH1 released an increasing number of infectious virions (**Fig. 5A**), whereas the cluster mutants (4Bmt1, 4Bmt2, and 4Bmt3) produced no detectable infectious virions. For all these mutants, no HCV antigens were detected by immunoblotting in transfected cells (Core, NS4B, and NS5A were tested; data not shown). The cluster mutants were defective for virus replication. We then concentrated on the first N-terminal cluster and created single alanine substitution mutants for the three hydrophobic residues, W43A, V46A, and W50A, because the cluster was considered

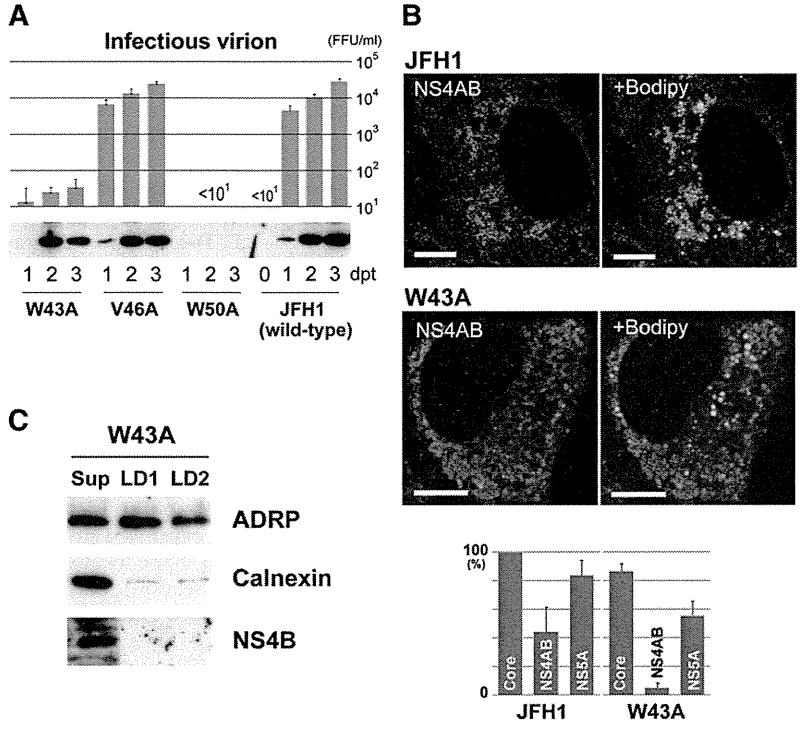

Fig. 5. JFH1 mutants harboring single alanine substitutions for hydrophobic residues of NS4B are defective for replication. (A) Effect on virus replication of alanine substitutions in NS4B region of JFH1. (Top) Titration of infectious virions released from transfectants of JFH1 or mutant RNAs. Culture supernatant of each transfectant was assayed for infectivity at the indicated days post transfection (dpt). FFU, focus forming unit. Mean values from three or four independent experiments are shown; error bars denote SD. (Bottom) Expression of NS4B in the transfectants of JFH1 or mutant RNAs. (B) Localization of HCV antigens and the changes caused by W43A mutation. (Top) Change in localization of NS4AB (NS4B and/or NS4A). Transfectants with JFH1 or W43A RNA were stained with anti-NS4AB antibody, followed by staining with Bodipy 493/503. Scale bars, 10 μm. (Bottom) Comparison of LD association for HCV antigens between W43A- and JFH1-RNA-transfected cells. The percentages of positive cells for LD association of each antigen are shown. When association was seen for at least six LDs in a section, the transfectant was counted as positive. Mean values from three independent experiments are shown; error bars denote SD. (C) Localization of NS4B to LD preparations obtained from W43A-RNA-transfected cells. LD fractions were prepared and analyzed as in Fig. 2, right.

to be most effective for LD targeting of NS4B as described above. When RNAs were transfected into Oc cells, the mutants released different numbers of infectious virions (Fig. 5A). As compared with wild-type, W43A released only 1/300 to 1/1,000 of infectious virions, and V46A released comparable amounts of virions. W50A released no detectable infectious virions. Interestingly, W43A mutant, as well as V46A, expressed comparable amounts of HCV antigens as did wild-type, as confirmed by immunoblotting (Fig. 5A). In contrast, expression of HCV antigens was negligible for W50A (only faint bands were seen with longer exposure; data not shown). Although the W50A mutant was of interest to clarify the mechanisms of the defect, further analysis was not performed.

We then analyzed by confocal microscopy LD targeting of NS4B for W43A mutant, comparing it with that of the wild-type (Fig. 5B and supplementary Fig. V). We could not obtain antibodies for immunofluorescent detection of JFH1 NS4B; therefore, we used anti-NS4AB polyclonal antibody, which reacted with both NS4A and NS4B proteins. Distributions of NS4B (and/or 4A) and other antigens were observed by confocal microscopy for transfectants of wild-type and W43A (Fig. 5B and supplementary Fig. V). For JFH1, NS4B (and/or 4A) showed a reticular staining pattern, but a considerable amount of stain was concentrated around LDs and some showed broken (incomplete) ring-shape staining surrounding the LDs. In contrast, for W43A, NS4B (and/or 4A) showed a reticular pattern or small bubble-shape staining, but the stain had no relation to the LDs. Core protein showed clear ring-shape staining at the margins of the LDs in both wild-type (supplementary Fig. V) and W43A. However, for the latter, there was a slight increase in the percentage of transfectants without ring-shape staining of Core (but with reticular pattern alone). NS5A showed the staining patterns seen for both the Core and NS4AB. For both wild-type (supplementary Fig. V) and W43A, we observed clear or broken ring-shape staining surrounding the LDs, and the stain concentrated around LDs. We also tried imaging with anti-NS3 and anti-NS5B antibodies, which were used for immunoblotting of JFH1 antigens; however, the results of staining were not informative. The percentages of transfectants positive for LD association of antigens were compared for wild-type and W43A (Fig. 5B, bottom). In W43A, LD association of NS4B (and/or 4A) was markedly decreased as compared with wild-type, whereas

that of Core and NS5A was mildly decreased. For V46A mutant, percentages of positive transfectants were 97, 28, and 79%, for Core, NS4AB, and NS5A, respectively.

Finally, we purified LD fractions from W43A transfectant and analyzed for HCV antigens by immunoblotting (Fig. 5C and supplementary Fig. VI). In contrast to LD fractions from wild-type (supplementary Fig. II), calnexin content in LD1 and LD2 was comparable, suggesting that the W43A mutation in NS4B affects membrane micro-architecture around LDs. This suggestion was supported by drastic changes in distribution of NS4B (and/or 4A) around LDs, where it seemed as if the distribution pattern of the ER membranes themselves was altered by the mutation of NS4B (Fig. 5B). In both LD1 and LD2, NS4B was not detected by immunoblotting, suggesting that NS4B harboring the W43A mutation could not interact with LDs (Fig. 5C). The other HCV antigens, NS3, NS5A, and NS5B, were detected in both LD1 and LD2 (supplementary Fig. VI). Also in W43A, the Core protein was not detected in LD fractions but in the ultracentrifugation pellet.

DISCUSSION

In the present study, we demonstrated that HCV NS4B has the ability to target LDs. In the imaging analysis using Cherry constructs, some expressed NS4B showed ring-shape structures at the margins of LDs, suggesting that NS4B was present near to LD membranes. This was confirmed by the colocalization results of NS4B with ADRP in ring-shape structures. Biochemical approaches also showed LD targeting of NS4B. It was important to establish whether LD targeting of intact NS4B protein occurred in the presence of other HCV proteins, because the HCV proteins, including NS4B, physically and functionally interact with each other during virus replication. To clarify this, we used OR6 cells in which genome-length HCV-O RNA was stably replicating, hence, functional HCV proteins were present. We found that NS4B existed in the crude LD fraction (LD1 in Fig. 2, right), suggesting that NS4B was localized to the membranes associated with LDs. Analysis of LD fractions from JFH1-RNA-transfected cells also suggested that NS4B localized to such LD-associated ER membranes rather than on the LD surface membranes themselves (supplementary Fig. II).

In cellular LD-targeting proteins, the targeting mechanism is thought to be complex and multifactorial (1). However, two major required features of amino acid sequence have been proposed: one is the amphipathic α-helix (19–23), and the other is a rather undefined hydrophobic region (24–26). Some LD-targeting proteins, such as caveolin-1 and associated with lipid droplet protein 1 (ALDI) (24, 42), showed dual localization to LDs and ER in relation with cellular lipid dynamics. One simple explanation may be that the LD-targeting sequences also have ER-targeting activity. LD biogenesis is believed to be initiated from the accumulation of lipids between the two membrane leaflets of the ER (1–3); therefore, another explanation is that proteins initially target the ER membranes and are then assorted on the emerging LD membranes by lateral diffusion with the aid of additional, yet undefined mechanisms. The latter targeting model has also been proposed for the HCV Core, in which the truncated form of the Core protein targets LDs more efficiently (22). However, this LD-assorting mechanism is unlikely for NS4B, because NS4B has at least four transmembrane helices by which the protein is integrated into the ER bilayer membrane (43). It should be noted that LDs are surrounded by lipid monolayers. Taking together the proposed sorting mechanisms of other LD-targeting proteins with the result that LD-targeting sites were present in each cytosolic domain, a likely model is that NS4B is present in the ER and that both cytosolic terminal domains interact simultaneously with the LD surface membrane through the hydrophobic residues in amphipathic helices; NS4B tethers or catches the emerging LDs on or very near to the ER (**Fig. 6**). The results from biochemical analysis of LD preparations, in which NS4B seemed to be present in LD-associated membranes rather than on the LD surface membranes themselves, support this model. To clarify whether NS4B and ADRP were present in the identical membrane structure, we also performed fluorescence recovery after photobleaching (FRAP) analysis at the site of colocalization of Cherry-4B1–261 and EGFP-ADRP. Unfortunately, definitive data have not been obtained, because of the time resolution constraints of our equipment. We think that further investigation is needed to prove our hypothesis.

Our imaging study also revealed that hydrophobic residues in amphipathic helices [43W, 46L (V in JFH1), 50W, 57F, 61I, and 64L in the N-terminal domain; 242V, 246L, 249L, and 253I in the C-terminal domain] were important for LD targeting of NS4B. Mutational study of these residues in JFH1 replication/infection system revealed their role in LD targeting by NS4B and the significance of LD targeting in replication of infectious virions. The cluster mutants (three or four residues simultaneously mutated to alanine) were defective in virus replication. The amphipathic helices are multifunctional; for example, they are involved in oligomerization of NS4B (31, 44), formation of membranous web (31, 44) and replication complex (31, 45), and membrane association (40, 41). Therefore, multiple inhibitory mechanisms may be acting in the cluster mutants to cause severe defects.

Examination of single alanine substitution mutants focused on the residues in the first cluster (W43, V46, and W50) and clarified their role in virus replication. The results from W43A and W50A mutants indicated that both tryptophan residues are critical for the production of infectious virions. In contrast to W43A, the W50A mutant severely impaired the expression of HCV antigens. This might have resulted from a severe defect in RNA replication, or the residue 50W might be involved in the synthesis or processing of HCV polyproteins or in protein stability, in addition to known functions in NS4B. The defective mutant W43A was key to demonstrating the relationship between the hydrophobic residues and LD targeting of NS4B and the significance of LD targeting in virus replication. As shown in Fig. 5, we could not detect LD association of W43A NS4B, indicating that disruption of LD association of NS4B resulted in reduced

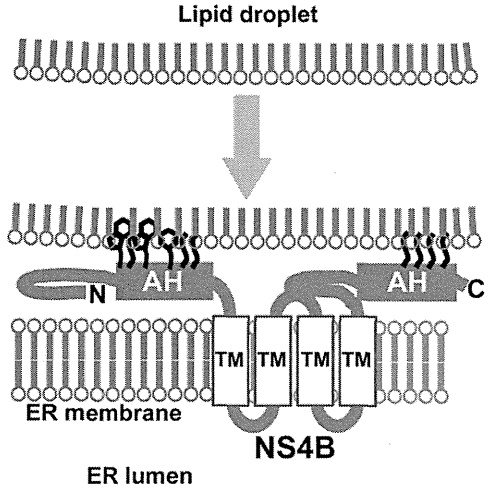

Fig. 6. Schematic representation of the hypothetical role of NS4B. NS4B tethers LDs on ER through the hydrophobic residues in the amphipathic helices (AH). N and C indicate the N- and C-terminal of NS4B, respectively. TM, transmembrane helix.

infectious virion release. This conclusion was supported by the results for V46A mutant, in which LD association of NS4B was apparently not affected and infectious virion release was comparable to that of wild-type JFH1. The residue 46V might not be important for LD targeting in strain JFH1.

In contrast to the JFH1 system, the impact of W43A mutation was unclear from the overexpression results using a truncated form of NS4B (Fig. 4). According to our model (Fig. 6), NS4B mediates association of LDs with ER membranes. When LDs move away from the site of association, a large force may act to disrupt the interaction between NS4B and LD membranes, and the residue 43W may be important to maintain the interaction as it is highly hydrophobic. The interactions of each of the hydrophobic residues involved in LD targeting depend on the adopted conformations of NS4B and those of molecules interacting with NS4B (HCV proteins, cellular proteins, or lipids); the changes in the mutual positioning of these molecules can induce steric hindrance. The 43W residue might be critical in such microenvironments. In contrast, the truncated form of NS4B (amino acids 1–73) may target LDs directly in a less regulated manner. This interaction may not be related to ER membranes and, hence, may not be affected by LD movements. The 43W residue influence is less than that of the intact NS4B.

We used an anti-NS4AB antibody; therefore, it remains to be resolved which antigens were observed in our imaging study (Fig. 5B and supplementary Fig. V). NS4A is a small protein consisting of 54 amino acids and is closely associated with NS3 to form NS3–4A complex. NS3–4A complex is thought to associate with ER membranes through the N-terminal hydrophobic α-helix of NS4A as a membrane anchor (46). Thus, it is unlikely that the W43A mutation of NS4B directly elicits solely the loss of association between NS3–4A and LDs as seen in Fig. 5B. At present, it is also not known whether the NS3–4A complex has an activity by itself to target LDs, although NS3 harbors an amphipathic helix α_0 that mediates membrane association (46). The most straightforward interpretation is that both NS4B and NS4A (and NS3) are present on ER membranes close to LDs, via the function of NS4B, and that W43A mutation causes loss of association with (or proximity to) LDs of both these proteins (but mostly NS4B).

The reason why LD targeting by NS4B is critical for virus replication is of interest. The microenvironment of LDs and ER membranes is thought to initiate HCV virion assembly, in which the nascent genome meets and associates with the Core protein to form nucleocapsids (10). Upon or after capsid formation, some particles may acquire an envelope (47), probably by utilizing ER membranes containing envelope proteins. Simultaneously, the virions might associate (or be coated) with components resembling VLDL, such as triglycerides, probably supplied from LDs, and apolipoproteins to become lipoviroparticles. Although the process of lipoviroparticle formation remains unclear, NS4B may function to establish such a microenvironment. NS4B can undergo a major conformational change, in which the N-terminal domain translocates to the luminal side of the ER (43), suggesting that the LD-targeting domain is masked by this event. The translocation was reduced in the presence of NS5A (48), suggesting a functional switch for NS4B. NS4B is indeed multifunctional because of its amphipathic helices, and in addition, it is thought to interact with other NS proteins (49), to hydrolyze GTP (50), and to modulate lipid metabolism (51). It is, therefore, of particular interest how, when, and where these activities have emerged and been regulated. A simple explanation may be that each activity simply emerges depending on the position or location of the NS4B molecule and what exists around it. The amphipathic helices of NS4B may function as ER anchors, as long as LDs are not present near the ER.

The authors thank Drs. K. Shimizu, Y. Shimotai, M. Hijikata, and T. Hayashida for valuable comments. Technical assistance by K. Toyosawa is gratefully acknowledged.

REFERENCES

1. Digel, M., R. Ehehalt, and J. Füllekrug. 2010. Lipid droplets lighting up: insights from live microscopy. *FEBS Lett.* **584:** 2168–2175.
2. Beller, M., K. Thiel, P. J. Thul, and H. Jäckle. 2010. Lipid droplets: a dynamic organelle moves into focus. *FEBS Lett.* **584:** 2176–2182.
3. Ohsaki, Y., J. L. Cheng, M. Suzuki, Y. Shinohara, A. Fujita, and T. Fujimoto. 2009. Biogenesis of cytoplasmic lipid droplets: From the lipid ester globule in the membrane to the visible structure. *Biochim. Biophys. Acta.* **1791:** 399–407.
4. Miyanari, Y., K. Atsuzawa, N. Usuda, K. Watashi, T. Hishiki, M. Zayas, R. Bartenschlager, T. Wakita, M. Hijikata, and K. Shimotohno. 2007. The lipid droplet is an important organelle for hepatitis C virus production. *Nat. Cell Biol.* **9:** 1089–1097.
5. Kato, N., M. Hijikata, Y. Ootsuyama, M. Nakagawa, S. Ohkoshi, T. Sugimura, and K. Shimotohno. 1990. Molecular cloning of the human hepatitis C virus genome from Japanese patients with non-A, non-B hepatitis. *Proc. Natl. Acad. Sci. USA.* **87:** 9524–9528.
6. Tsukiyama-Kohara, K., N. Iizuka, M. Kohara, and A. Nomoto. 1992. Internal ribosome entry site within hepatitis C virus RNA. *J. Virol.* **66:** 1476–1483.
7. Tanaka, T., N. Kato, M. J. Cho, and K. Shimotohno. 1995. A novel sequence found at the 3′ terminus of hepatitis C virus genome. *Biochem. Biophys. Res. Commun.* **215:** 744–749.